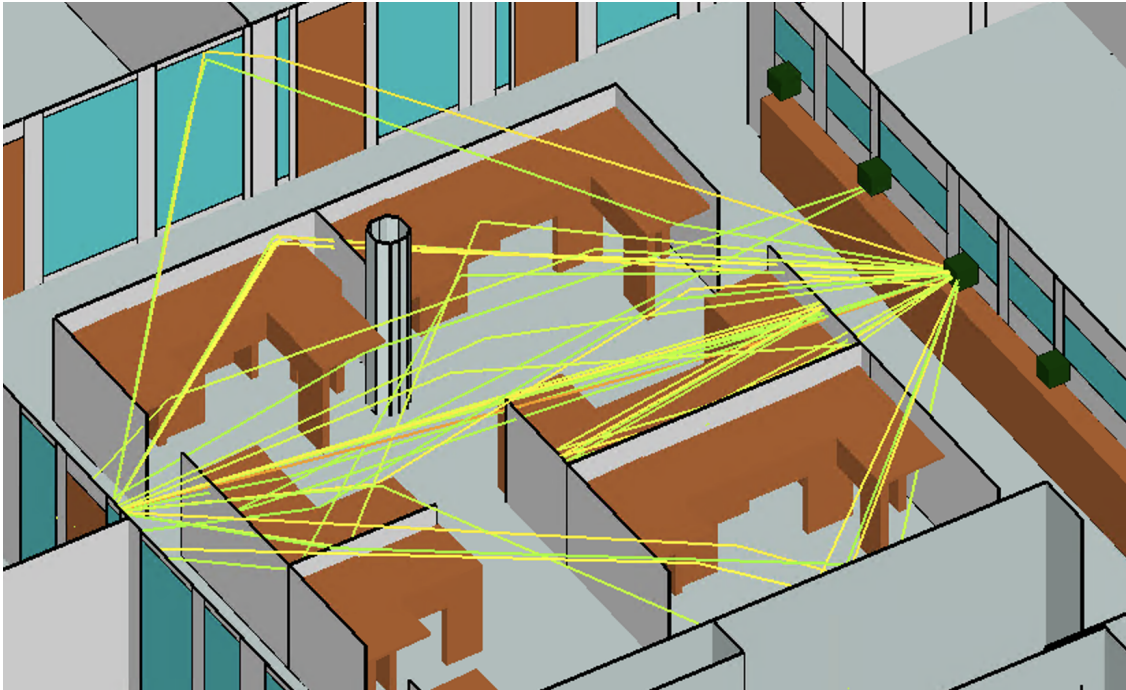




CHALMERS
UNIVERSITY OF TECHNOLOGY

MASTER'S THESIS 2021



Simulations of the Capacity and Coverage for a Multi-User Distributed MIMO Network

Master's Thesis in Microtechnology and Nanoscience

Simon Rimborg
Emma Rådahl

Department of Microtechnology and Nanoscience
CHALMERS UNIVERSITY OF TECHNOLOGY
Gothenburg, Sweden 2021

MASTER'S THESIS 2021

Simulations of the Capacity and Coverage for a Multi-User Distributed MIMO Network

Simon Rimborg, Emma Rådahl



CHALMERS

Department of Microtechnology and Nanoscience
CHALMERS UNIVERSITY OF TECHNOLOGY
Gothenburg, Sweden 2021

Simulations of the Capacity and Coverage for a Multi-User Distributed MIMO Network

Simon Rimborg, Emma Rådahl

© Simon Rimborg, Emma Rådahl, 2021.

Supervisor: Christian Fager, Department of Microtechnology and Nanoscience
Thomas Eriksson, Department of Electrical Engineering
Husileng Bao, Department of Microtechnology and Nanoscience
Examiner: Christian Fager, Department of Microtechnology and Nanoscience

Master's Thesis 2021
Department of Microtechnology and Nanoscience
Chalmers University of Technology
SE-412 96 Gothenburg
Telephone +46 31 772 1000

Cover: Simulated office environment showing the propagation path to one receiver point from one transmitter antenna that is part of a distributed MIMO network. Image produced in the simulation software Wireless InSite.

Typeset in L^AT_EX
Gothenburg, Sweden 2021

Simulations of the Capacity and Coverage for a Multi-User Distributed MIMO Network

Simon Rimborg, Emma Rådahl
Department of Microtechnology and Nanoscience
Chalmers University of Technology

Abstract

An ever growing increase of connected devices and data rates around the world needs to be met by new communication technologies. Using an antenna array with multiple antennas, a so-called MIMO system, has proven to be a successful way to boost the capacity of wireless communication systems. By spatially separating the antennas to cover a larger area, while still being carefully synchronised to a central unit, many unwanted effects in a MIMO system such as shadowing and spatial correlation can be mitigated. This is the idea of a distributed MIMO (D-MIMO) system. The potential of D-MIMO has been observed in other studies and testbed applications. Proving that a D-MIMO system can be reliably and accurately simulated would enable a cheap and time-effective way to further investigate the capabilities and development of new D-MIMO systems.

This project investigated the similarities and differences between a real D-MIMO system and a simulated D-MIMO system by comparing simulated data to measured data obtained from a testbed. After showing that simulations can be a reliable way to study D-MIMO, further investigations were carried out. The thesis shows an overall higher capacity for a D-MIMO system compared to a regular co-located MIMO (C-MIMO) system. For an indoor office environment it is shown that similar capacity can be reached when using 12 transmitter antennas for C-MIMO as with 7 transmitter antennas for D-MIMO. Further simulations were made comparing higher mmWave signal frequencies, which still showed D-MIMO being advantageous compared to C-MIMO. However, the higher frequency simulations also showed a less stable system for both C-MIMO and D-MIMO. Lastly, outdoor simulations were made that can be recreated and confirmed with a testbed in a future project. The outdoor simulations also show a higher capacity for the D-MIMO system compared to the C-MIMO system.

Overall, the results show that a D-MIMO system can be created in a simulated environment which is important for further investigating the capabilities of future D-MIMO system deployments. It is also shown that the D-MIMO system is superior to an ordinary C-MIMO system with regards to received power, coverage and capacity.

Keywords: distributed, MIMO, multi-user, cell-free, simulation, capacity, mmWave.

Acknowledgements

We would like to express our sincere thanks to Christian Fager who throughout this project has given us of his time and helped us move forward. Your enthusiasm has been an inspiration. For being a helpful source of knowledge, we would like to thank Thomas Eriksson who has guided us from the start. We would also like to thank Husileng Bao for his invaluable patience and helpfulness when answering our countless questions. Finally, we would like to thank the personnel at Remcom for teaching us the software Wireless InSite. Especially we would like to thank Tarun Chawla and Sam Magliaro who went above and beyond with providing us with useful files, tips and answers to all of our questions.

Simon Rimborg and Emma Rådahl, Gothenburg, June 2021

Contents

List of Figures	xiii
List of Tables	xvii
List of Abbreviations	xix
1 Introduction	1
1.1 Aim	2
1.2 Project Specification	2
1.3 Previous Projects	3
1.4 Contributions	3
1.5 Limitations	4
1.6 Report Structure	5
2 Theory	7
2.1 Wireless Channel	7
2.1.1 Frequency and Wavelengths	8
2.1.2 Multiple Access	9
2.1.3 Duplexing	10
2.1.4 Channel Matrix	10
2.2 MIMO	11
2.2.1 Singular Value Spread	12
2.3 Capacity in a MIMO System	13
2.4 Distributed and Cell-Free MIMO	15
2.5 Antennas	16
2.5.1 Omnidirectional Antennas	17
2.5.2 Patch Antennas	17
2.6 Propagation Modeling Software	18
3 Method	21
3.1 Testbed and Measurements	21
3.1.1 Hardware	21
3.1.2 Measurements and Signal Processing	22

3.2	Simulations in Wireless InSite	23
3.2.1	Floor Plan and Features	23
3.2.2	Materials	24
3.2.3	Waveforms	26
3.2.4	Antennas	26
3.2.5	Transmitters	27
3.2.6	Receivers	29
3.2.7	Study Area	29
3.2.8	Communication Systems	30
3.2.9	Output	31
4	Indoor Environment	33
4.1	Received Power	33
4.1.1	Resulting Received Power for Each Receiver Point	33
4.2	Singular Value Spread	34
4.2.1	CDF of Singular Value Spread	35
4.3	Capacity	36
4.3.1	User Capacity per Position	37
4.3.2	Histogram of the Sum Capacity	38
4.4	Antenna Removal	39
4.4.1	Sum Capacity for Each Antenna Combination	39
4.4.2	Capacity Decrease From Removal of Antennas	42
4.4.3	Antennas Present When Achieving Above Average Sum Capacity	42
4.5	Discussion	43
5	Frequency Comparison	45
5.1	Received Power	45
5.1.1	Comparison Between the Received Power	45
5.2	Singular Value Spread	47
5.2.1	Distribution of Singular Value Spread	47
5.3	Capacity	47
5.3.1	User Capacity per Position	47
5.3.2	Histogram of Sum Capacity	48
5.4	Discussion	48
6	Outdoor	51
6.1	Received Power	51
6.1.1	Heatmap of Power and Received Power per Position	51
6.2	Singular Value Spread	52
6.2.1	CDF of Singular Value Spread	53
6.3	User Capacity	53
6.3.1	User Capacity per Position	54
6.4	Sum Capacity	54
6.4.1	Histogram of the Sum Capacity	54
6.5	Antenna Removal	55

6.5.1	Sum Capacity All Combinations of Antenna- and User Combinations	55
6.6	Discussion	56
7	Conclusion	59
	Bibliography	61
A	Example Output from Wireless InSite	I
B	Complement to Indoor Environment Study	V
B.1	Received Power Without Phase	V
B.2	Sum Capacity With Different SNR	VI

List of Figures

2.1	Wireless communication system. The wireless channel is what the transmitted signal, x , propagates through.	7
2.2	MIMO communication system. Every receiver receives a signal from each transmitters.	8
2.3	From left to right: TDMA, FDMA and CDMA illustrated. TDMA separates the channels in time slots, FDMA separates the channel between frequencies and CDMA separates the channels using coding schemes.	9
2.4	Illustration for the principles of frequency division duplex (left) and time division duplex (right).	10
2.5	Illustration of the power allocation technique referred to as water filling. Each bar represents one subchannel with a individual SNR, λ . The height of each bar is $1/\lambda_m$, a low bar indicates a sub channel with a high SNR. The power allocated to each subchannel is the difference between the constant power level $1/\lambda_0$ and the top of the bar. A channel with better conditions receives more power than a channel with bad conditions.	14
2.6	Illustration of the difference between C-MIMO (a) and D-MIMO (b). Different colours represent different cells. For C-MIMO, the antennas are placed on the same location and from there serve the users located within the given cell. For D-MIMO the APs are distributed at different locations within the cell, all connected to its cell's central unit.	16
2.7	The cells are formed around the individual user. The user can connect to APs using different CUs.	16
2.8	(a) The antenna pattern of a omnidirectional antenna generated by Wireless InSite. (b) photo of the omnidirectional antenna used as receiver in the testbed.	17
2.9	(a) The antenna pattern of a patch antenna generated by Wireless InSite. (b) photo of the patch antenna used as transmitter in the testbed.	18

3.1	Schematic overview of the testbed. The CU consists of a PC which generates the signal. The signal is converted to an optical signal via an FPGA and an E/O converter. Optical fibers carry the signal to the APs. The APs convert the optical signal to an electrical signal which is then filtered and amplified before being transmitted. The receiver antenna is placed on a robot and can give CSI to the PC via wi-fi.	22
3.2	A screen snippet showing the multiple tabs (Waveforms tab highlighted) in Wireless InSite main view. The tabs are: Images, Features, Materials, Waveforms, Antennas, Transmitters/Receivers, Study area, Communication systems, and Output.	23
3.3	The built model of the office environment for the indoor simulation. Area A refers to a kitchen and conference area and B refers to an open office area. The images are from Wireless InSite.	24
3.4	The built model for the outdoor simulation. The model includes buildings (white/grey) and terrain (green). The images are from Wireless InSite.	24
3.5	The waveform properties window in Wireless InSite for the pulse shape root-raised cosine. The window shows the chosen parameters along with a plot of the resulting shape. The chosen parameters are a carrier frequency of 2.365 GHz, pulse width of 0.2 μ s and a roll-off factor of 0.2. The phase and pulse repetition frequency are default values.	26
3.6	Images showing the placements of transmitters for both (a) C-MIMO and (b) D-MIMO in the indoor environment. The placement is according to the their respective locations during the testbed measurements.	28
3.7	Images showing the placements of transmitters for both C-MIMO and D-MIMO for the outdoor simulation. The arrows in (b) indicate the directions of the antennas.	28
3.8	Images showing both (a) the robot trajectory during the measurements and (b) the grid of receiver points used in the simulation. . . .	29
3.9	Images showing both (a) a possible trajectory for future measurements and (b) the grid of receiver points for the outdoor simulation. . .	30
4.1	Total received power at each receiver location from both C-MIMO and D-MIMO transmit antennas with center frequency of 2.365 GHz.	34
4.2	Showing the difference in order of magnitudes of the singular values before and after the constant is multiplied. The x-axis refers to the subchannel from the different transmitter antennas. Note the change on the y-axis. (a) Singular values before multiplied with a constant factor. (b) Singular values after multiplying the channel matrix with a constant factor of 5,000.	35
4.3	A CDF showing the singular value spread for C-MIMO and D-MIMO from both measurements and simulation. A small spread is close to 0 dB.	36

4.4	Boxplot showing the user capacity for each location containing all 135,751 combinations in the case of 4 users being placed at the 44 positions.	37
4.5	Histogram showing the sum capacities for C-MIMO and D-MIMO. . .	38
4.6	Graph showing the average sum capacity for all user and antenna combinations for both C-MIMO and D-MIMO. The x-axis is all different antenna combinations with a decreasing number of antennas. Change in number of removed antennas is represented by the dashed lines. The size of each interval is dependent on the number of combinations, presented in Table 4.1. The y-axis is the average of the total sum capacity for all user combinations. The darker lines show the mean in each interval. (a) Average sum capacity for all user combinations versus every antenna configuration. (b) Showing the same as Fig. 4.6a but zoomed in to show the first 350 antenna combinations.	40
4.7	Boxplot showing the average sum capacity for all user and antenna combinations for both C-MIMO and D-MIMO. The x-axis shows the number of antennas removed. The y-axis is the average of the total sum capacity for all user combinations with the red line being the median.	41
4.8	Boxplot showing the probability of a C-MIMO system and D-MIMO system to achieve a reference capacity with different number of antennas removed. The x-axis shows the number of antennas removed and the y-axis is the probability with the red line being the median. .	42
4.9	Boxplot of the occurrence of each antenna in the configurations that provide an above average sum capacity in the D-MIMO system in percent. Each box represents the occurrence in percent of one specific antenna in the above average antenna configurations.	43
5.1	Heat maps over the office area for C-MIMO using a center frequency of 2.365 GHz and 28 GHz.	46
5.2	Heat maps over the office area for D-MIMO using a center frequency of 2.365 GHz and 28 GHz.	46
5.3	Total received power for each receiver point. The dashed lines illustrate the median of the received power calculated in Watts.	46
5.4	A CDF showing the distribution of singular value spread for C-MIMO and D-MIMO for both 2.365 GHz and 28 GHz. The singular value spread is calculated for all possible user combinations among the 44 receiver points. A small spread is close to 0 dB.	47
5.5	Boxplot showing the user capacity for each location in the case of 4 active users. Every position is represented with a blue box where the top and bottom of the box represents 75th and the 25th percentiles of the capacity, respectively. The red line is the median capacity and the dashed tails extends to the maximum and minimum capacity, not including outliers.	48
5.6	Histogram with the sum capacity calculated for all possible user combinations for (a) 2.365 GHz and (b) 28 GHz.	49

6.1	Heat maps of the outdoor environment for both C-MIMO and D-MIMO when using a center frequency of 2.365 GHz. The antenna positions can be found in the pink circles. The range is between -120 dBm (purple) to -45 dBm (red).	52
6.2	Total received power at each receiver location from both C-MIMO and D-MIMO transmit antennas with center frequency of 2.36 GHz from the outdoor simulation.	52
6.3	A CDF showing the singular value spread for C-MIMO and D-MIMO from the outdoor simulation. A small spread is close to 0 dB.	53
6.4	Boxplot showing the user capacity for each location in the case of 4 users in an outdoor environment.	54
6.5	Histogram showing the sum capacities for C-MIMO and D-MIMO in the outdoor simulation.	55
6.6	Boxplot showing the average total sum capacity for all user and antenna combinations for both C-MIMO and D-MIMO. The x-axis shows the number of antennas removed. The y-axis is the average of the total sum capacity for all user combinations with the red line being the median.	56
B.1	The received power for the indoor environment when not including the phase.	V
B.2	The sum capacity shown with different SNR values.	VI

List of Tables

3.1	Table showing all materials used in the simulations along with their respective properties and the assigned feature. All materials are specified for a frequency of 2.4 GHz or 28 GHz, depending on the simulation. When available, the materials are based on the ITU recommendations and are found in the material library provided in Wireless InSite. The permittivity is specified relative to free space permittivity and is therefore unit less. For conductivity, the values presented are first for 2.365 GHz and then 28 GHz.	25
3.2	Chosen antenna parameters for the different simulations.	27
3.3	Table showing the chosen input parameters for the study area for both the indoor and outdoor simulations.	30
4.1	The different number of possible antenna combinations when using different number of active antennas.	39

List of Abbreviations

AP	Access points
BS	Base station
C-MIMO	Co-located multiple-input multiple-output
CDF	Cumulative distribution function
CDMA	Code division multiple access
CSI	Channel state information
CSIR	Channel state information at receiver
CSIT	Channel state information at transmitter
CU	Central unit
D-MIMO	Distributed multiple-input multiple-output
DL	Downlink
FDD	Frequency division duplex
FDMA	Frequency division multiple access
FPGA	Field-Programmable Gate Array
ITU	International Telecommunication Union
LoS	Line of sight
MIMO	Multiple-input multiple-output
MISO	Multiple-input single-output
mmWave	millimeter wave
MU-MIMO	Multi-user multiple-input multiple-output
RoF	Radio-over-fiber
SDoF	Sigma-delta-over-fiber
SIMO	Single-input multiple-output
SISO	Single-input single-output
SNR	Signal-to-noise ratio
SVD	Singular value decomposition
TDD	Time division duplex
TDMA	Time division multiple access
UL	Uplink
USRP	Universal software radio peripheral
VSWR	Voltage standing wave ratio
ZFBF	Zero-forcing beamforming

1

Introduction

Society today is dependent on wireless communication; ranging from mobile phones and computers to smart homes and self driving cars. The technologies are constantly evolving to keep up with the ever increasing demand for higher data rates and connectivity. With 5G being deployed around the world, the next generation of communication systems are being researched and tested.

Multiple input multiple output (MIMO) is a technique widely used today in wireless communication in order to increase the capacity of the communication systems by using more antennas [1]. While MIMO systems in general are providing larger capacity compared to, for example, single input single output (SISO) systems [2], there is still room for improvement. For future generations of mobile networks a different structure of the MIMO systems is being studied, namely distributed MIMO (D-MIMO) and creation of so called cell-free systems [3].

Higher frequencies, namely millimeter wave (mmWave) frequencies, are of interest for use in 5G due to the limitation of available frequency resources in the lower frequency bands [4]. However, the ability for a electromagnetic waves to propagate large distances and through objects decrease at higher frequencies. By distributing the antennas, as in a D-MIMO system, the probability of a signal needing to propagate a large distance or through multiple objects decreases.

D-MIMO differs from regular co-located MIMO (C-MIMO), which is the standard for MIMO systems, in that with D-MIMO the antennas are not on the same base station (BS), but rather spread between different access points (APs) that are connected and collaborating through a central unit (CU) [3]. These distributed and synchronised APs can still technically be seen as one giant MIMO BS [5], but does not to the same extent suffer from C-MIMO related issues such as spatial correlation and shadowing [3]. Connecting the APs to a CU is not limited to a single BSs, but a D-MIMO “BS” can replace one or multiple C-MIMO BSs [5].

The concept *cell-free massive MIMO* extends the idea of a D-MIMO system and can be divided into three parts in order to get a better understanding of what it means. First, MIMO implies using multiple antennas on the transmitter side and/or receiver side in order to increase the capacity and hence data rates [6]. In general, a multi-user MIMO system is assumed for these applications, meaning multiple

receivers/users with one or multiple antennas instead of a single user with multiple antennas. Secondly, massive MIMO introduces the idea of increasing the number of antennas in the transmitter significantly to further increase capacity [7]. Finally, the term cell-free refers to a D-MIMO network where cells are formed around the user instead of being fixed around base stations [8]. This dynamic approach has the potential to improve the performance since the most beneficial AP connection can be prioritised and the user will not experience negative cell edge effects [9]. In short, cell-free massive MIMO refers to a network where a large number of physically distributed APs serve a smaller number of users. The cells are formed dynamically around the users instead of as geographical cells around the BSs.

In order to meet the increasing demands for capacity and data rates for future mobile networks, a distributed antenna system joint with massive MIMO is an interesting idea [10], [11]. To test the concept Chalmers University of Technology, hereafter referred to as Chalmers, has developed a testbed where D-MIMO experiments can be made to measure the potentials and limitations of a cell-free network [12].

The following sections in this chapter will introduce the scope of the thesis. First, the project is specified by defining the overall aim followed by a specification of the different issues that is to be investigated. Then, the previous works that lay base for this thesis and the contributions of this thesis are stated. Lastly, the limitations of this project are presented.

1.1 Aim

The aim of this project is to analyse the potential and capacity limits of D-MIMO in comparison to traditional C-MIMO through simulations. The main part is to create a simulated environment that corresponds to the real life environment where measurements were made with the testbed.

Once confirmed that the simulated environment characteristics are similar to the real life environment further investigations will be made. The aim of these investigations is to analyse the effect when using different transmit frequencies, study the effect of varying the number of antennas included in the system, and also when testing in a different environment.

1.2 Project Specification

Real measurements have been made at Chalmers with the developed testbed and the task is to, on the basis of these measurements, analyse the performance of such a system through simulations. The measurements emulate a multi-user MIMO system downlink scenario: a base station consisting of 12 transmitter antennas transmitting to 4 users. The transmitter antennas are movable in order to create both a C-MIMO and a D-MIMO system. The software Wireless InSite [13] will be used to create simulated environments and to perform the simulations. The first task is

to create the simulated environment and examine how accurate the simulations are compared to the testbed measurements. The similarities between the measurements and simulations will be evaluated by comparing received power throughout the 44 receiver locations, comparing singular value spreads and comparing capacities.

The following task includes studying the effect of different antenna configurations for the systems and examining how robust the systems are for removal of antennas. This will be done by removing the contribution from different antennas in Matlab and observing how the capacities are affected.

Further simulations will also be made using a different frequency than what is used in the testbed measurements. This task will compare the systems for transmit signals using higher frequencies with the purpose of studying the effect of using mmWaves frequencies, namely 28 GHz. Once again, studies of these simulations will include comparing C-MIMO and D-MIMO regarding received power, singular value spreads and capacities. Similarities and differences between the different frequency options will also be studied.

Finally, there will also be simulations made in a different simulated environment. The task is to investigate how the C-MIMO and D-MIMO systems compare in other environments beyond the indoor office environment. The area of choice for the outdoor simulation is a pedestrian area between university buildings at Chalmers, with coordinates $57^{\circ}41'32.2''\text{N}$ $11^{\circ}58'31.6''\text{E}$, which is small enough to be recreated with the testbed in a future project. The studies of these simulations will include comparing C-MIMO and D-MIMO regarding received power, singular value spreads and capacities. Also, similarities and differences between the indoor- and outdoor environments will be studied.

1.3 Previous Projects

The thesis is based on previous projects conducted at Chalmers. Specifications of the testbed for the D-MIMO system are presented in [12] and [14]. The 12 microstrip patch antennas used as transmitters in the testbed were built as a Master's Thesis project and are presented in [15]. The testbed measurements that were used as comparisons are presented in [16].

1.4 Contributions

This thesis will provide an understanding of the reliability and accuracy of simulating D-MIMO communication systems. It will be shown through simulations how C-MIMO and D-MIMO systems compare to each other regarding received power throughout an area, singular value spread and capacity. Further on, it will compare the effect different antenna configurations have on C-MIMO and D-MIMO systems. Initial studies regarding D-MIMO using mmWave frequencies and in an outdoor scenario are also accounted for.

1.5 Limitations

The data used in this thesis as comparison has been gathered with the developed testbed and is therefore limited to the specifications used there. The hardware specific limitations include a center frequency of 2.365 GHz, bandwidth of 5–20 MHz, and offline signal processing.

The amount of previous existing measurement data used for evaluating the results of the office environment simulations is limited. The data available for this project is from a single measurement session on a downlink transmission, which makes it the only point of reference for the given environment, and the reliability of the simulations is based on the reliability of that measurement session. The set of data includes testbed measurements from 44 different receiver locations for both C-MIMO and D-MIMO. The data from the measurements that are relevant are in the form of channel matrices, one for C-MIMO and one for D-MIMO. Since there is only measurement data from one environment, the results from any additional simulation can not be confirmed by measurements at this point. The reliability will be based on the accuracy of the first simulation.

Due to limitation in time it will not be possible to make further indoor measurements with the testbed to confirm the simulated results when changing antenna configurations. Neither will it be possible to do outdoor measurements to recreate the outdoor simulations.

The simulations will be limited to the technical specifications of the software used. The level of detail of the environments is limited due to time; a trade-off between how similar the measurements and simulations are compared to how long it takes to recreate the environment in the software must be made.

When analysing the data, the system is assumed to fulfill the following properties:

- perfect channel state information in the transmitter
- the signal is in the high SNR region
- all transmitter antennas have the same output power
- interference between antennas is negligible.

When comparing the different systems, only the technical performance aspect will be considered. The practicality or cost of implementation is not an aspect that will be taken into account in this project.

The 28 GHz frequency simulations will not be analysed regarding antenna placement. This is due to a limitation in time. The choice of analysing antenna placement for 2.365 GHz was made since this can more easily be confirmed using the testbed in future projects.

The system that will be considered is a downlink BS scenario. Therefore, other types of MIMO systems will not be covered in this project. Henceforth, when referring to a MIMO systems only base station scenarios are implied.

1.6 Report Structure

This report will first, in Chapter 2 present the relevant theory that is needed to understand the results. Chapter 3 will account for how the measurements that are to be simulated were performed. In the same chapter the process of building the simulation environment will be presented. Chapter 4 will consist of the indoor study. This includes simulated results compared to the measurements along with a study of the effect of removing antennas in the different systems. After this, in Chapter 5, a comparison will be made between using 2.365 GHz and 28 GHz as a center frequency in an indoor environment. Then, in Chapter 6, results from simulating a outdoor environment will be presented. The report will end with a summarising conclusion, Chapter 7.

2

Theory

The following chapter introduces the theory necessary to understand and interpret the results presented in Chapter 4–6. First, the theory concerning wireless communication, MIMO systems and antennas is given. Further on, the signal propagation software that is used for the simulation is presented.

2.1 Wireless Channel

A wireless channel is constantly changing and even more so in an urban environment such as in the middle of a large city [17, pp. 6–8]. Changes in the channel can for instance appear when the transmitter or receiver is moved, when objects are moved which blocks the signal or when a surface on which the signal reflects moves. The variation in the signal strength due to blockage and objects is referred to as shadowing. The changes can affect the received signal's time of arrival, frequency, phase and power [17, ch. 3].

The channel can mathematically be explained as

$$y = Hx + n, \quad (2.1)$$

where y is the received signal, x is the transmitted signal, H represents the channel and n is noise. This channel and communication system is illustrated in Fig. 2.1.

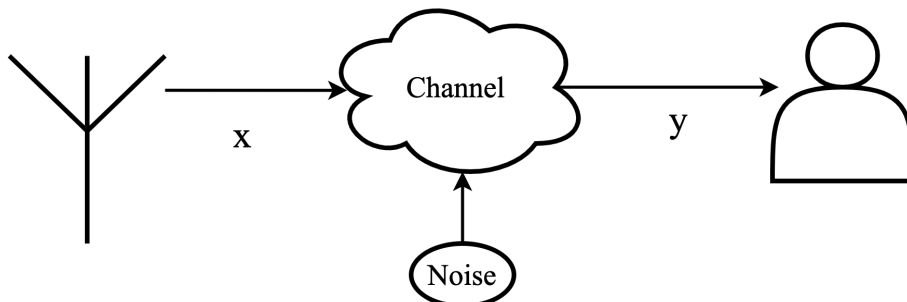


Figure 2.1: Wireless communication system. The wireless channel is what the transmitted signal, x , propagates through.

A system with M_t transmitter antennas and M_r receiver antennas, i.e. a MIMO system, has multiple channels and the variables in (2.1) become vectors and matrices to reflect the multiple antennas, as shown with bold letters in

$$\mathbf{y} = \mathbf{H}\mathbf{x} + \mathbf{n}, \quad (2.2)$$

where \mathbf{y} and \mathbf{n} are vectors of size $M_r \times 1$, \mathbf{H} is a $M_r \times M_t$ channel matrix and \mathbf{x} is a $M_t \times 1$ vector [17, pp. 321–323]. A MIMO system is illustrated in Fig. 2.2 where 4 APs are communicating with 3 users.

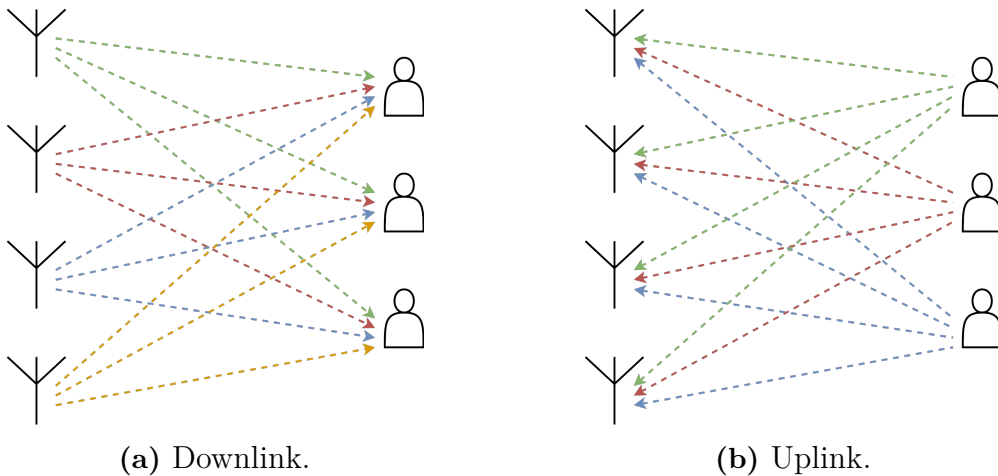


Figure 2.2: MIMO communication system. Every receiver receives a signal from each transmitters.

When a BS is transmitting to a user/receiver the transmission is referred to as downlink (DL). This is illustrated in Fig 2.2a where multiple antennas on, for example a BS, is transmitting to the users. Contrary to this is when the user is transmitting to the BS, this transmission is referred to as uplink (UL), seen in Fig 2.2b.

Since the wireless channel is not constant, the communication systems can not be pre-configured to compensate for the channel changes. To mitigate the channel effects the channel must be estimated and then compensated for. Knowledge of the channel effects is called channel state information (CSI). CSI at the receiver side (CSIR) can be achieved by using known pilot bits in the message [18]. With feedback to the transmitter CSI at the transmitter (CSIT) is achieved and much of the channel effects can be compensated for using precoding [17, ch. 10]. Precoding is further explained in Section 2.2

2.1.1 Frequency and Wavelengths

A wireless signal is often described by its frequency and the cellular network is divided into different bands that correspond to different frequencies [19]. Today, most of the frequency bands are occupied and are an expensive resource [4]. The 4G network operates on frequencies below 6 GHz [19]. New for 5G is the use of

mmWave frequencies, i.e. 10 GHz and above [4]. The wavelength, λ , is calculated as

$$\lambda = \frac{c}{f}, \quad (2.3)$$

where c is the speed of light and f is the frequency of the signal [17]. A radio wave with lower frequency can propagate a longer path compared to a radio wave with higher frequency [20], but the use of higher frequencies can yield higher data rates because of the more available bandwidth [21, pp. 173–178].

2.1.2 Multiple Access

Multiple access is a technique required when multiple users want to share a channel medium [17, pp. 454–459], [21, pp. 120–123]. This can be achieved by separating the channel in, for example, time, frequency or with orthogonal codes. These multiple access techniques are called time-, frequency- and code division multiple access (TDMA, FDMA and CDMA) respectively. The different multiple access techniques are illustrated in Fig. 2.3.

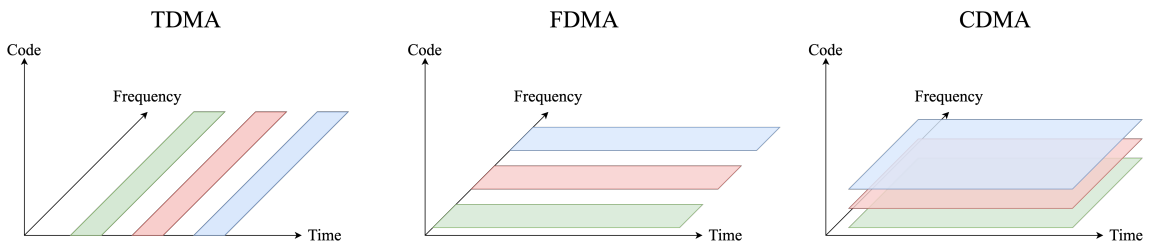


Figure 2.3: From left to right: TDMA, FDMA and CDMA illustrated. TDMA separates the channels in time slots, FDMA separates the channel between frequencies and CDMA separates the channels using coding schemes.

With TDMA the users are assigned different time slots during which the entire channel bandwidth is dedicated to the user. The transmitter and receiver cycles through the different slots in repetitive order and hence the channel is split in time. To avoid interference guard time is added between the slots.

In FDMA the channel’s bandwidth is divided into smaller channels. This way the users have their own channel they can communicate within. To be able to implement non-ideal filters the channels needs to be separated with with guard bands. This way the users have their own channel they can communicate within continuously.

For CDMA neither time nor frequency is divided between the users. Instead, the signals are divided using a coding scheme. By using orthogonal codes the signals are separated and the users can utilise the same frequency spectrum at the same time.

2.1.3 Duplexing

A technique referred to as duplexing has to be implemented for a device to be able to both transmit and receive [22]. There are two kinds of duplexing, namely half duplex and full duplex. With full duplex the communication equipment can receive and transmit simultaneously. Half duplex implies that communication can be made in both directions but only in one direction at a time.

Duplexing can be implemented as frequency division duplex (FDD) or time division duplex (TDD). For FDD the channel bandwidth is divided in two bands, one band for up-link and one for down-link, and for TDD the channel is divided in time slots. The division of the two methods are shown in Fig 2.4.

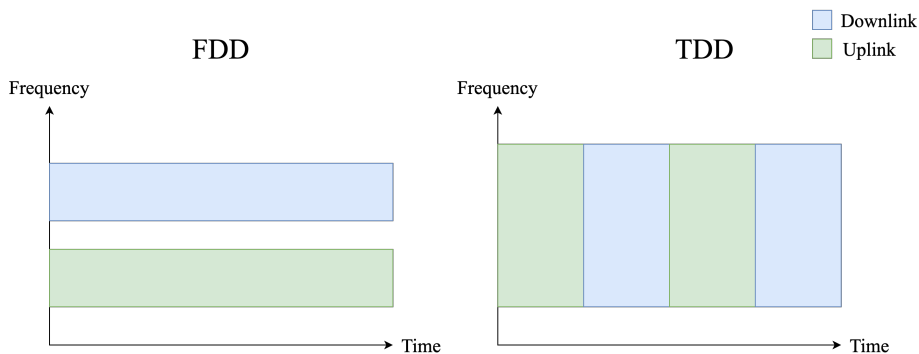


Figure 2.4: Illustration for the principles of frequency division duplex (left) and time division duplex (right).

2.1.4 Channel Matrix

The channel matrix, \mathbf{H} , describes the gain in the wireless channel and the effect it has on the transmitted signal [17, pp. 321]. The channel matrix can be estimated in order to use a technique called precoding. Precoding is useful in order to mitigate channel effects on the transmitted signal and is further explained in Section 2.2. There are several methods to estimate the channel matrix. One method is to transmit a known signal and comparing the received data with the known signal. This known signal is typically referred to as pilot data. Based on (2.2) the channel matrix can be estimated by a least square method as

$$\hat{\mathbf{H}} = (\mathbf{x}^* \mathbf{x})^{-1} \mathbf{x}^* \mathbf{y}, \quad (2.4)$$

where \mathbf{x} is the transmitted data, the asterisk denotes the hermetian transpose, \mathbf{y} is the received data and $\hat{\mathbf{H}}$ is the channel estimate [16], [23].

The simulations do not transmit a certain message but instead evaluate the propagation of the electromagnetic wave. The channel matrix in this project can therefore

not be estimated using pilot data, as in (2.4). The channel matrix is instead estimated using the impulse response of the system. Each element in the channel matrix is calculated as

$$\hat{\mathbf{H}}_{M_r, M_t} = \sum_{k=1}^{N_{paths}} G_k e^{j\phi_k}, \quad (2.5)$$

where $\hat{\mathbf{H}}_{M_r, M_t}$ is the gain of the channel from transmitter M_t to receiver M_r . N_{paths} is the number of recorded paths between M_t and M_r , ϕ_k is the phase of each path and G_k is the magnitude of the path gain for the field and is given in dB. The linear gain, G_k , is calculated as

$$G_k = \sqrt{\frac{P_{RX}}{P_{TX}}}, \quad (2.6)$$

where the received power, P_{RX} , of path k and transmitted power, P_{TX} , are in Watts.

So in a simulated scenario (2.5) can be used to calculate the channel matrix, but for a real life scenario pilot data is used as in (2.4).

2.2 MIMO

A communication system where both the transmitter and receiver are equipped with multiple antennas is referred to as a MIMO system. There are some special cases for MIMO, for instance: when there are multiple antennas only at the transmitter or receiver, the system is called a MISO or SIMO system, respectively. Also, if the transmitter and receiver only have one antenna each, this is referred to as a SISO system.

For cases where a transmitter with multiple antennas is communicating with multiple receivers each having one or multiple antennas, this is referred to as multi-user MIMO (MU-MIMO). MU-MIMO is an implementation of multiple access, as described in Section 2.1.2 for MIMO. When the number of transmit antennas are much larger than the number of receive antennas, this system is referred to as massive MIMO [7].

For a MIMO system, two types of gain can be achieved compared to a SISO system, namely diversity gain and spatial multiplex gain [17, pp. 334–335, 340]. Diversity gain is achieved when the number of antennas is larger than the number of users and can also be applicable to a SIMO or MISO system. For a SIMO and MIMO system, the signal received at each antenna can be added together to increase the received signal power. With suitable combining techniques the signal to noise ratio (SNR)

at the receiver can be improved. For a MISO and MIMO system, the antennas can transmit the same signal to minimise the chance of the signal being blocked or interfered. Also, for a MIMO and MISO system with CSIT a technique called beamforming can be applied. With beamforming the transmit antennas send the signal in such a way that the electromagnetic waves of the signal create constructive interference at the receiver, thus increasing the received signal power.

By enabling independent transmission over parallel channels the data rate is increased by using the same time and frequency resources. This technique is referred to as spatial multiplex gain and it can be applied in a MIMO system when there is CSIT [17, pp. 340]. The technique uses precoding at the transmitter and de-coding at the receiver to emulate M parallel SISO channels, where $M \leq \min(M_t, M_r)$. For this technique the channel matrix is decomposed by 3 different matrices using singular value decomposition (SVD) as

$$\mathbf{H} = \mathbf{U}\mathbf{\Sigma}\mathbf{V}^* \quad (2.7)$$

where \mathbf{U} and \mathbf{V} are unitary matrices of size $M_r \times M_r$ and $M_t \times M_t$ respectively and $\mathbf{\Sigma}$ is a $M_r \times M_t$ rectangular diagonal matrix consisting of the singular values, σ , of \mathbf{H} . The number of singular values in $\mathbf{\Sigma}$ is equal to $\text{rank}(\mathbf{H})$. The asterisk denotes the Hermetian of the matrix.

Using the SVD of the channel matrix, the equation of the received message can be written as

$$\begin{aligned} \mathbf{y} &= \mathbf{H}\mathbf{x} + \mathbf{n} \\ &= \mathbf{U}\mathbf{\Sigma}\mathbf{V}^*\mathbf{x} + \mathbf{n}. \end{aligned} \quad (2.8)$$

By precoding the signal, $\tilde{\mathbf{x}}$, with \mathbf{V} the signal can be written as $\mathbf{x} = \mathbf{V}\tilde{\mathbf{x}}$, and shaping the received signal, \mathbf{y} , with \mathbf{U}^* as $\tilde{\mathbf{y}} = \mathbf{U}^*\mathbf{y}$. It can be seen in

$$\mathbf{U}^*\mathbf{y} = \mathbf{U}^*\mathbf{U}\mathbf{\Sigma}\mathbf{V}^*\mathbf{V}\tilde{\mathbf{x}} + \mathbf{U}^*\mathbf{n}. \quad (2.9)$$

Since \mathbf{U} and \mathbf{V} are unitary matrices, i.e. $\mathbf{U}\mathbf{U}^* = \mathbf{V}\mathbf{V}^* = \mathbf{I}$, parallel SISO channels are theoretically achieved since $\mathbf{\Sigma}$ is a diagonal matrix as seen in

$$\tilde{\mathbf{y}} = \mathbf{\Sigma}\tilde{\mathbf{x}} + \tilde{\mathbf{n}}. \quad (2.10)$$

2.2.1 Singular Value Spread

The singular values, σ , found in the diagonal singular value matrix $\mathbf{\Sigma}$ can be used to calculate the singular value spread. The singular value spread is a metric of how

large the difference of performance is between the different parallel channels from (2.10) [24]. From (2.10) it can be seen that transmitted signal is scaled by the singular values of the channel, i.e. a small singular value indicates a weak received signal and a large singular value indicates a strong received signal. Hence, a large singular value spread means a large variation in signal quality between the different MIMO subchannels. The singular value spread can be expressed as

$$S = \frac{\left(\prod_{m=1}^M \sigma_m^2\right)^{\frac{1}{M}}}{\frac{1}{M} \sum_{m=1}^M \sigma_m^2}. \quad (2.11)$$

Here, the singular value spread, S , is the ratio between the geometric mean and the arithmetical mean, where σ_m is the singular value for a specific sub channel, m , and M is the number of parallel channels.

As can be seen in (2.11) the numerator will be close to σ_m^2 if the singular values are similar but will be smaller than σ_m^2 if the singular values are different. The same goes for the denominator; if the singular values are similar the denominator will be close to σ_m^2 but smaller than σ_m^2 if the singular values differ. However, the nominator will shrink faster compared to the denominator if the singular values are different since it takes the product instead of the sum. Hence, for a channel with similar singular values, which means that the system provides an equal channel to all user, the fraction will yield a value close to 1. For cases where the singular values are different, which means that there is a large difference between the best and worst channel, the fraction will decrease.

2.3 Capacity in a MIMO System

Capacity is a measure of the maximum data rate that can be transmitted over a channel with an arbitrary small bit error rate [17, pp. 99], [21, pp. 166–167]. In this section, three capacity measures will be accounted for: the user capacity, sum capacity and channel capacity. The user capacity in a MIMO system is a metric of the rate of data that can be transmitted to one user per channel use in the system. The user capacity is dependent on the individual channel between the transmitter and a specific user, so it can therefore be large variations in user capacity between users. By taking the sum of all user capacities in the system, the sum capacity can be calculated. The sum capacity is the maximum total data rate for all users. The sum capacity is a measure of the throughput for the system per unit frequency. The channel capacity is a measure of the maximum rate of information possible over the entire channel.

In the high SNR region it can be assumed that all subchannels have good conditions for communication and therefore it is optimal to transmit with full power on all channels. However, with low or highly varying SNR this is not the optimal method. With low SNR there is a need to apply, so called, water filling [17, ch. 4]. Water filling is a power allocation technique that aims to utilise the channels with good conditions to achieve higher data rates [25],[17, ch. 4]. The concept is illustrated in

Fig. 2.5. The bars in the figure refer to different subchannels with varying SNR, λ . The constant power level is the “water level”, which in the figure is marked as $1/\lambda_0$. The allocated power to each channel is the difference between the water level and the top of each bar, $P_m = 1/\lambda_0 - 1/\lambda_m$.

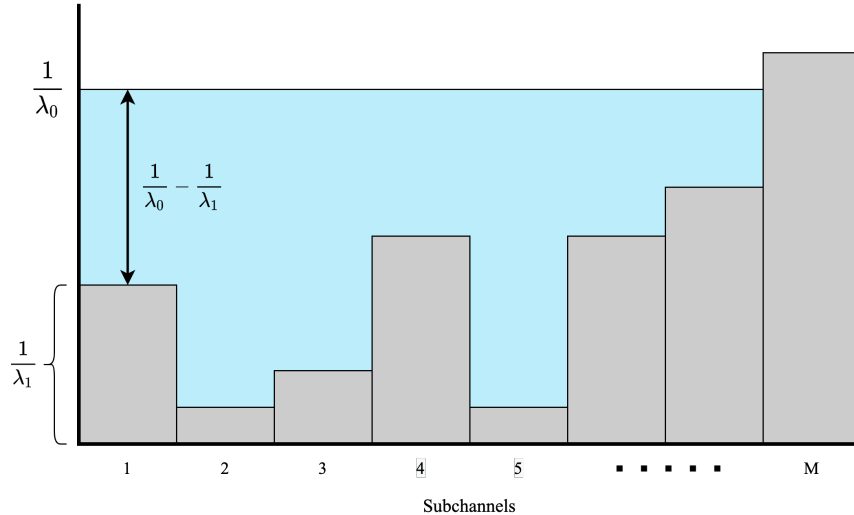


Figure 2.5: Illustration of the power allocation technique referred to as water filling. Each bar represents one subchannel with a individual SNR, λ . The height of each bar is $1/\lambda_m$, a low bar indicates a sub channel with a high SNR. The power allocated to each subchannel is the difference between the constant power level $1/\lambda_0$ and the top of the bar. A channel with better conditions receives more power than a channel with bad conditions.

In this project it is assumed that the system operates in the high SNR region and therefore close to the optimal capacity is achieved by transmitting with the equal power in all transmitters.

The expression for the capacity in a multi-user system originates from the Shannon-Hartley theorem, seen in

$$C = B \cdot \log_2(1 + \text{SNR}) \quad (2.12)$$

where C denotes the capacity over the entire channel and B the bandwidth of the channel. As stated in [25] the user capacity is a measure of the maximum possible data rate of a single user per channel use and could therefore be written as

$$C_m = \log_2 \left(1 + \frac{P_{rm}}{BN_0} \right). \quad (2.13)$$

Here, C_m denotes the user capacity for user m , $\frac{P_{rm}}{BN_0}$ is the SNR for user m , where P_{rm} is the received signal power for user m . This measure is per unit frequency so the logarithm is not multiplied with the bandwidth as in (2.12) and the unit is bits/s/Hz.

Since high SNR is assumed and also that all antennas are identical and assumed to transmit with equal power the received power for user m , P_{rm} , can be written as

$$P_{rm} = \sigma_m^2 \frac{P}{n_T} = \sigma_m^2 P_{tx} \quad (2.14)$$

where σ_m is the singular value for subchannel m , P is the total transmitted power and n_T is the number of transmitters [25]. P_{tx} denotes the transmitted power for one channel. By combining (2.13) and (2.14), the user capacity can be expressed as

$$C_m = \log_2 \left(1 + \sigma_m^2 \frac{P_{tx}}{BN_0} \right). \quad (2.15)$$

The user capacity is dependent on the individual channel and therefore varies depending on the individual user. A measure of the capacity for all subchannels users is referred to as sum capacity and according to [25] is expressed as

$$C_{sum} = \sum_{m=1}^{n_{users}} \log_2 \left(1 + \sigma_m^2 \frac{P_{tx}}{BN_0} \right). \quad (2.16)$$

The capacities of each active subchannel are added together. However, since the power is assumed to be equal the only varying factor is σ_m^2 .

Both the user capacity and the sum capacity are given in unit frequency, the unit is bits/s/Hz. However, to express the sum rate capacity for the entire channel the expression (2.16) is multiplied with the bandwidth as

$$C = B \sum_{m=1}^{n_{users}} \log_2 \left(1 + \sigma_m^2 \frac{P_{tx}}{BN_0} \right) \quad (2.17)$$

where the sum rate capacity, C , is given in bits/s. In this project the results are calculated using (2.15) and (2.16).

2.4 Distributed and Cell-Free MIMO

C-MIMO means that all the transmit antennas are placed on the same unit and is the most common type of MU-MIMO system. Here, a coverage area, a so-called cell, is formed around the MIMO transmitter and all the transmit antennas serve the users located inside that given cell. However, this method has its shortcomings such as cell-edge effects, spatial correlation and shadowing [5]. A way to mitigate this is to implement, so called, D-MIMO.

Instead of having the antennas placed in the same spatial location, they are distributed in the cell but carefully synchronised to a central unit [26]. This difference between C-MIMO and D-MIMO is shown in Fig. 2.6. By having the antennas separated, the issue of spatial correlation and shadowing is addressed. The spatial spread of antennas increases the independence of the different channels which results in a smaller singular value spread and higher performance. The spread also reduces the effect of shadowing due to the fact that a larger diversity in channels increase the chance of a line of sight (LoS) connection [3], [27]. The channels can thus be considered to be independent since they are not interfering with each other [3], [28]. The power of a signal in the wireless channel is decreasing polynomially with the distance which causes a drop in performance at the cell edge [26]. However, in a

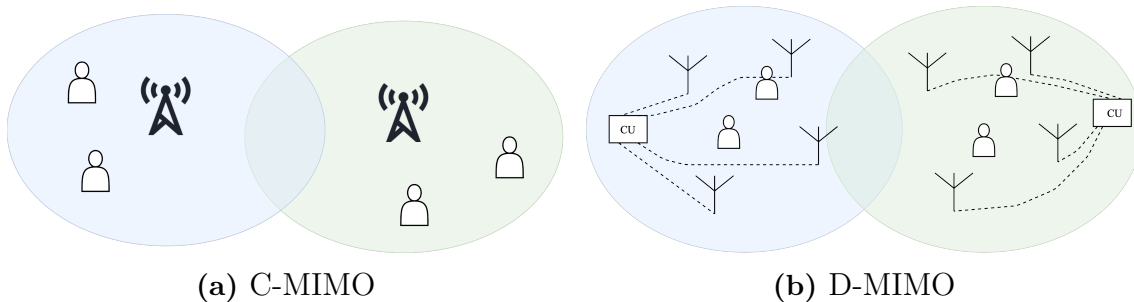


Figure 2.6: Illustration of the difference between C-MIMO (a) and D-MIMO (b). Different colours represent different cells. For C-MIMO, the antennas are placed on the same location and from there serve the users located within the given cell. For D-MIMO the APs are distributed at different locations within the cell, all connected to its cell’s central unit.

distributed system it is more likely that the distance between the user and the APs is shorter than in the co-located system [27].

One area of use for a distributed system is implementation of cell-free massive MIMO. This refers to the removal of traditional cells that are used in C-MIMO and D-MIMO. Instead of having geographically stationary cells around APs, the cells are formed around the user and connect to the antennas in a dynamical manner, as illustrated in Fig. 2.7. This is done by having a large number of APs serving a much smaller number of users with the same time- and frequency resource. The user can connect to APs using different CUs. The channel state information is gathered by using TDD [3], [9].

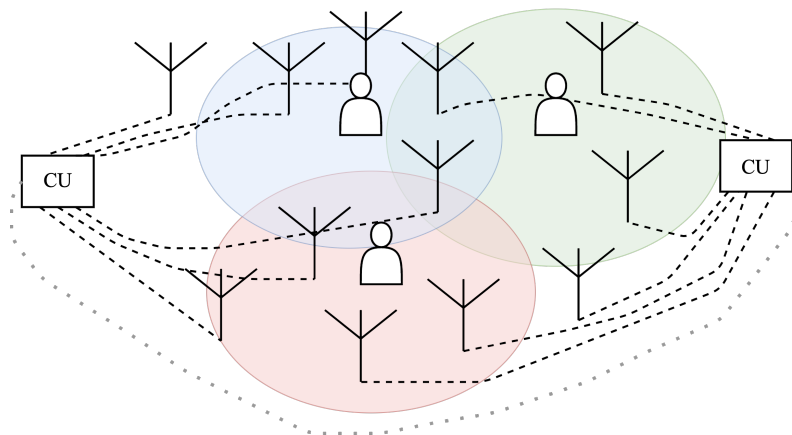


Figure 2.7: The cells are formed around the individual user. The user can connect to APs using different CUs.

2.5 Antennas

In a wireless communication system the antennas are one of the main components. An antenna’s gain is the measure of the ability of radiating the input power in a

specific direction: a high gain implies a higher efficiency in utilising the power and a low gain implies a lower efficiency [29]. The gain, G of an antenna is the product of the antenna's directivity, D , and efficiency, ϵ , as shown in

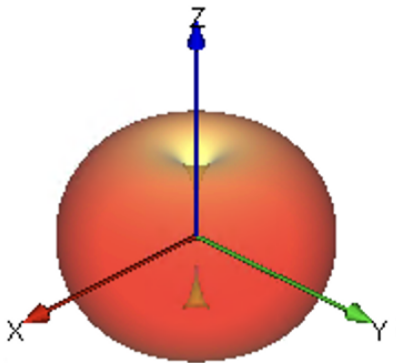
$$G = \epsilon D. \quad (2.18)$$

The directivity of the antenna is defined in a specific direction and relative to a uniform directivity obtained with an isotropic antenna. The directivity of an antenna is often illustrated as an antenna- or radio pattern. The efficiency is defined as the radiated power from the antenna divided by the input power to the antenna.

In the following two sections the antennas that are used in the testbed are accounted for. For the transmitters 12 rectangular patch antennas were used and for the receiver one omnidirectional antenna was used.

2.5.1 Omnidirectional Antennas

An omnidirectional antenna has a radio pattern that spans 360 degrees in the horizontal plane and is in the shape of a torus. This provides coverage in the horizontal plane but the antenna has little to no gain in the vertical direction. Example of an antenna pattern of an omnidirectional antenna can be seen in Fig. 2.8a. The omnidirectional antenna used as a receiver in the testbed was VERT2450 [30]. A photograph of this antenna is shown in Fig. 2.8b.



(a) Antenna pattern.



(b) VERT2450.

Figure 2.8: (a) The antenna pattern of a omnidirectional antenna generated by Wireless InSite. (b) photo of the omnidirectional antenna used as receiver in the testbed.

2.5.2 Patch Antennas

A patch antenna is an antenna in the form of a planar sheet of metal. Due to their shape they are space efficient and can easily be mounted on surfaces. A patch antenna is a, so called, directed antenna which radiates and/or receives more efficiently

in a specific direction. Example of an antenna pattern of a patch antenna can be seen in Fig. 2.9a. If an antenna is to be placed near a solid object a directional antenna can be beneficial to increase the gain in directions facing away from the solid object. A patch antenna used as transmitter in the testbed can be seen in Fig. 2.9b.

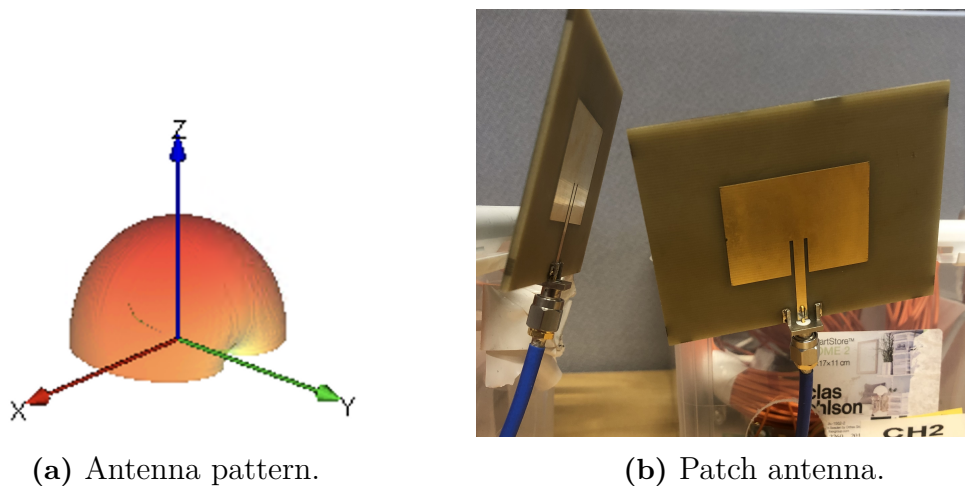


Figure 2.9: (a) The antenna pattern of a patch antenna generated by Wireless InSite. (b) photo of the patch antenna used as transmitter in the testbed.

The patch antennas used as transmitters in the testbed are 29.2×38.6 mm and were developed at Chalmers as part of a Master’s Thesis project [15].

2.6 Propagation Modeling Software

In a wireless communication system the signal propagates through the channel between the transmitter antenna to the receiver antenna. The propagation of these signals can be simulated to find a theoretical channel matrix. Examples of simple propagation modelling methods include theoretical and empirical models [31]. These models have a computational time that is faster but not as accurate compared to more advanced models. The empirical models also lack accuracy, especially for MIMO systems. Among the more advanced models are the ray tracing method, finite-difference time-domain method and method of moments, to name a few. These models require more computational time and resources. While the ray tracing method in many cases also requires more computational time, one of its benefits is that it can model using less computer resources compared to the other advanced models [31].

Ray tracing means that the electromagnetic wave is modeled as a ray. The ray will propagate through the simulated environment in a straight line and reflect, diffract and scatter on the present objects as per the user’s settings [31]. The method can be compared to how light waves (*rays*) from the sun (*transmitter antenna*) reflect, diffract and scatter before reaching your eye (*receiver antenna*).

The simulation software used in this project can model electromagnetic waves using ray tracing in full 3D. The software is called Wireless InSite and it is created by the company Remcom [13]. By using ray tracing Wireless InSite calculates the channel impulse response that is used to estimate the channel matrix, as in (2.5).

3

Method

This chapter includes description of the measurement process and the simulation process. First, the testbed is described regarding its hardware and software specifications. After this an account of how the measurements were carried out is presented. Following this is the simulation process in Wireless InSite. This describes how the simulations were carried out by presenting the chosen parameters and settings used to simulate C-MIMO and D-MIMO in both indoor and outdoor environments using 2.365 GHz and 28 GHz frequencies.

3.1 Testbed and Measurements

In order to examine D-MIMO and compare it with C-MIMO, a testbed was developed at Chalmers [12], [14] and measurements were made in an office environment [16]. The data from the measurements is used to compare the simulated C-MIMO and D-MIMO systems with the testbed's C-MIMO and D-MIMO systems.

3.1.1 Hardware

Figure 3.1 shows a schematic overview of this testbed structure. The two main parts are the central unit (CU) and the APs. Figure 3.1 also includes the receiver, which is not a fixed part of the testbed, but a necessity to measure the performance.

The testbed [12] uses a radio-over-fiber (RoF) technique called sigma-delta-over-fiber (SDoF) for transmission. SDoF is a technique that has proven to be a beneficial choice compared to analog- and digital-RoF [32]. The CU manages the digital processing and electrical to optical conversion. This is done by a sigma delta modulator in the PC, which forwards the signal to a Field-Programmable Gate Array (FPGA) and an electrical to optical converter. Twelve 30 m optical fibers carries the transmission to the APs where the signal is converted back from optical to electrical, carries out band pass filtering and amplifies the signal. In the case of measuring in the office environment, the receiver consists of a robot with an omnidirectional antenna [16]. This robot has the ability to follow a marked track, receive transmissions and transmit the data via WiFi to the central unit.

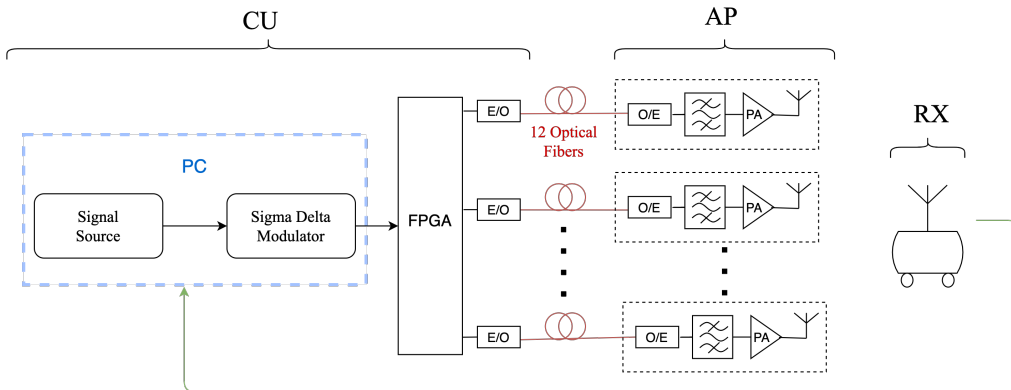


Figure 3.1: Schematic overview of the testbed [16]. The CU consists of a PC which generates the signal. The signal is converted to an optical signal via an FPGA and an E/O converter. Optical fibers carry the signal to the APs. The APs convert the optical signal to an electrical signal which is then filtered and amplified before being transmitted. The receiver antenna is placed on a robot and can give CSI to the PC via wi-fi.

3.1.2 Measurements and Signal Processing

The measurements that were conducted at Chalmers consist of 44 receiver locations in an indoor office environment [16]. For each receiver location a new channel estimation and a MISO communication is performed before the robot moves on to the next location. At the channel estimation stage, a known pilot was transmitted from the 12 APs to the receiver. Since the signal is known, adjustments such as central frequency compensation and timing adjustments are performed. After these adjustments, the preamble can be detected and the received signal is estimated to be as (2.2). The channel estimation is done by least square method, (2.4), where \mathbf{y} is the received signal and \mathbf{x} is the transmitted pilot.

At the communication stage CSIT precoding is applied. A technique called zero-forcing beamforming (ZFBF) is implemented in the testbed, however, in the case of a single receiver all precoders appear identical. Ideally, ZFBF would cancel out interference and the receiver would only receive the transmitted signal [33]. The formula for ZFBF can be written as

$$\mathbf{s} = (\hat{\mathbf{H}}\hat{\mathbf{H}}^*)^{-1}\hat{\mathbf{H}}\mathbf{x} \quad (3.1)$$

where $\hat{\mathbf{H}}$ is the estimated channel matrix, the asterisk denotes the hermetian, \mathbf{x} is the user data and \mathbf{s} is the transmitted data.

After the receiver has received the signal, offsets are again compensated for before the robot moves to the next location. Once the robot has moved to and stopped at the next location the process described in this section is repeated. Further information and a more detailed description of this process can be found in [12], [14] and [16].

3.2 Simulations in Wireless InSite

The process of simulating the propagation of electromagnetic waves in Wireless InSite consists of building a model of the given environment, specifying the elements that are to be included, and then setting the bounds and extent of the simulation. This section will present the process and settings for producing the simulated data used in Chapters 4–6.

The process of constructing an environment for simulation in Wireless InSite is divided into different individual parts, which is shown by the different tabs in Fig. 3.2. The settings from each tab will be presented in individual sections. For each individual section, the settings for the indoor simulations will be given first and for the outdoor simulations next. The Images and Features tab are combined into a single section called Floor plan and features and the Transmitter/Receiver tab is divided into two individual sections.

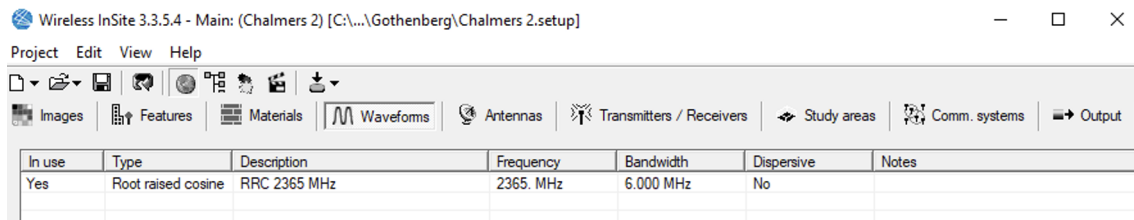


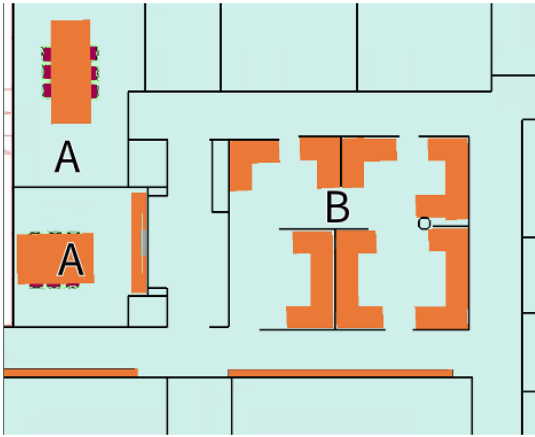
Figure 3.2: A screen snippet showing the multiple tabs (Waveforms tab highlighted) in Wireless InSite main view. The tabs are: Images, Features, Materials, Waveforms, Antennas, Transmitters/Receivers, Study area, Communication systems, and Output.

3.2.1 Floor Plan and Features

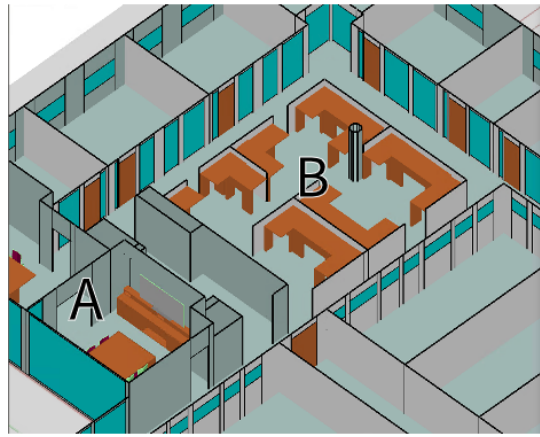
The first step is to build the floor plan, which is a representation of the indoor environment. This includes placing walls and features such as windows and doors. Wireless InSite is capable of importing a JPEG image of a floor plan that can be used for reference but can also import whole previously existing CAD-environments for a more accurate and detailed 3D model.

For the indoor simulations, objects such as the furniture are imported CAD-files in order to more accurately mimic the real office environment. The majority of the model was built by importing a JPEG image of the floor plan for an accurate placement of walls, windows, doors, etc. However, the features that were not included, for example the open office space between the corridors, were based on physical on-site measurements made with measuring tape.

Fig. 3.3 shows the built floor plan for the indoor model with the room from above in Fig. 3.3a and as a 3D-representation in Fig. 3.3b. The environment is divided into areas A and B. Area A is a kitchen and conference room area and B is an open office area. Hereafter, these areas will be referred to as areas A and B.



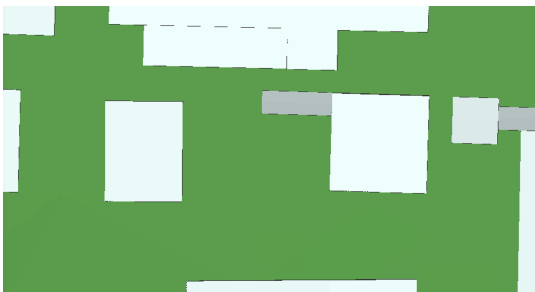
(a) Environment from above in 2D.



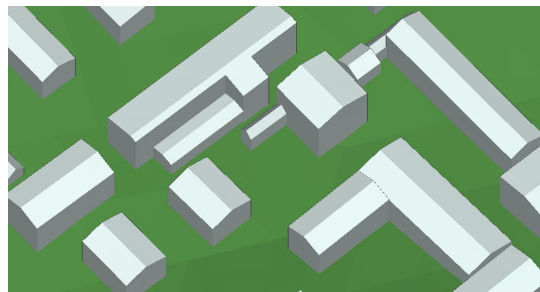
(b) Environment from above in 3D.

Figure 3.3: The built model of the office environment for the indoor simulation. Area A refers to a kitchen and conference area and B refers to an open office area. The images are from Wireless InSite.

For the outdoor simulation, OpenStreetMap [34] was used to create an accurate model of the terrain. This was to include aspects such as change in elevation etc. A model of the area was provided by Remcom which included the terrain and the nearby buildings. The model was imported into Wireless InSite and Fig. 3.4 shows the resulting model. The environment seen from above is shown in Fig. 3.4a and Fig. 3.4b is a 3D-representation of the same environment.



(a) Outdoor environment from above in 2D.



(b) Outdoor environment from above in 3D.

Figure 3.4: The built model for the outdoor simulation. The model includes buildings (white/grey) and terrain (green). The images are from Wireless InSite.

3.2.2 Materials

After the floor plan is built each feature and object in the floor plan is assigned a material. Wireless InSite provides a library of materials where each material is represented in a wide range of frequencies. When simulating with frequency 2.365 GHz, corresponding to the frequency of the measurements, materials specified at 2.4 GHz were used when available. When simulating with the 28 GHz waveform, materials specified for 28 GHz were used when available.

All materials used in the simulation are presented in Table 3.1 and are shown by different colors in Fig. 3.3b for the indoor environment and 3.4b for the outdoor environment. In Table 3.1 the properties for each material specified by the International Telecommunication Union (ITU) is presented. The walls in for the indoor environment are assigned two different materials; from table 3.1a Walls 1 refers to the outer walls and the walls surrounding area A, shown in a darker grey in Fig. 3.3b, while Walls 2 refers to the inner walls of the area in lighter grey. The doors in the floor plan are either opened or closed depending on their state during the real testbed measurements.

Table 3.1: Table showing all materials used in the simulations along with their respective properties and the assigned feature. All materials are specified for a frequency of 2.4 GHz or 28 GHz, depending on the simulation. When available, the materials are based on the ITU recommendations and are found in the material library provided in Wireless InSite [35]. The permittivity is specified relative to free space permittivity and is therefore unit less. For conductivity, the values presented are first for 2.365 GHz and then 28 GHz.

* For Wireless InSite the material Dry-Wall is specified as three layers. These are two layers of dry-wall, each with proprieties specified below, and in between a layer of free space.

** Metal and Foam are not ITU specific. Therefore, Metal does not have any specified valued assigned and Foam remains the same when increasing frequency.

(a) Indoor 2.365 GHz/28 GHz

Feature	Material	Permittivity	Conductivity [S/m]	Thickness [m]
Walls 1	Concrete	5.310	0.06622/0.4838	0.3
Walls 2	Dry-Wall*	2.940	0.02155/0.1226	0.0130
Ceiling	Ceiling board	1.5	0.001385/0.02413	0.00950
Floor	Concrete	5.310	0.06622/0.4838	0.3
Windows	Glass	6.270	0.01221/0.2287	0.003
Doors	Wood	1.99	0.01201/0.1672	0.03
Open doors	Free space	-	-	-
Tables	Wood	1.99	0.01201/0.1672	0.03
Bookcase	Wood	1.99	0.01201/0.1672	0.03
Chairs	Metal**	-	-	-
Chairs	Foam**	1.450	0.0002	0.04
TV-stand	Wood	1.99	0.01201/0.1672	0.03
TV-stand	Metal**	-	-	-

(b) Outdoor

Feature	Material	Permittivity	Conductivity [S/m]	Thickness [m]
Terrain	Dry Earth	3.0	0.001362	0
Buildings	Concrete	5.310	0.06622	0.3

3.2.3 Waveforms

The next step is to choose the waveform that is to be simulated. Based on the signal from the testbed measurements the chosen waveform is a root-raised cosine with carrier frequency of 2.365 GHz, pulse width of $0.2 \mu\text{s}$ and a roll-off factor of 0.2. This results in an effective bandwidth of 6 MHz. The settings and the resulting waveform is shown in Fig. 3.5. The phase and pulse repetition frequency settings are the default values.

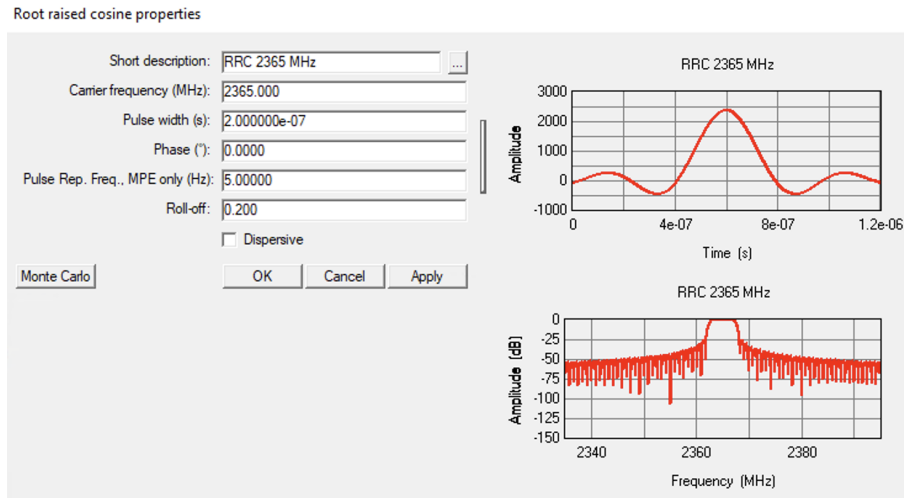


Figure 3.5: The waveform properties window in Wireless InSite for the pulse shape root-raised cosine. The window shows the chosen parameters along with a plot of the resulting shape. The chosen parameters are a carrier frequency of 2.365 GHz, pulse width of $0.2 \mu\text{s}$ and a roll-off factor of 0.2. The phase and pulse repetition frequency are default values.

To investigate how using mmWave frequencies affect the results, the same settings are applied with a change in carrier frequency to 28 GHz.

3.2.4 Antennas

As stated in Section 2.5, the simulations use two types of antennas; 12 rectangular patch antennas as transmitters and 1 omnidirectional antenna as a receiver. Wireless InSite provides both a library of antennas and the ability to import your own user defined antenna. For the user defined antennas the necessary parameters must be imported in order for Wireless InSite to properly create an antenna pattern.

The omnidirectional antenna was chosen from the provided library. The default values were selected apart from maximum gain that was set to 2.4 dBi and the voltage standing wave ratio (VSWR) that was set to 1.4, in accordance with the antennas' data sheet [30]. The chosen parameters are presented in Table 3.2a.

The patch antennas in the library did not offer flexibility in the rotation of the antenna, therefore a patch antenna with the setting shown in Table 3.2b was specified,

exported from Wireless InSite then imported as a user defined antenna. The resulting antenna pattern is shown in Fig. 2.8a and Fig. 2.9a for the omnidirectional antenna and patch antenna respectively.

When generating the results for mmWave frequencies, presented in Chapter 5, an omnidirectional antenna with Wireless InSite’s default values for 28 GHz was used as both transmitter and receiver antenna. The parameters are presented in Table 3.2a.

Table 3.2: Chosen antenna parameters for the different simulations.

(a) Table showing the chosen omnidirectional antenna parameters when using both 2.365 GHz and 28 GHz.

Antenna parameter	2.365 GHz	28 GHz
Maximum gain	2.4 dBi	0 dBi (default)
Polarisation	Vertical (default)	Vertical (default)
E-plane half-power beamwidth	90° (default)	90° (default)
E-plane first null beamwidth	180° (default)	180° (default)
Receiver Threshold	-250 dBm (default)	-250 dBm (default)
Transmission line loss	0 dB (default)	0 dB (default)
VSWR	1.4	1 (default)

(b) Table showing the chosen patch antenna parameters.

Antenna parameter	Value
Maximum gain	0 dBi (default)
Dielectric constant	4.4
Length	0.0386 m
Width	0.0292 m
Height	0.00157 m
Receiver Threshold	-250 dBm (default)
Transmission line loss	0 dB (default)
VSWR	1 (default)

3.2.5 Transmitters

The transmitter locations are placed in the floor plan and assigned antennas. The simulations are to include both C-MIMO and D-MIMO, therefore two different sets of 12 transmitter locations are used. Wireless InSite has a MIMO application that could be used for C-MIMO, however, the application can not handle a distributed antenna system. Therefore, in order to ensure equal post-processing of the results the built-in MIMO application is not used for C-MIMO. All transmitters for 2.365 GHz are assigned a patch antenna and for 28 GHz an omnidirectional antenna.

For the indoor simulations, the 12 transmitters for C-MIMO are placed together on top of a bookcase in two lines of 6 transmitters each at a height of 1.35 and 1.45 m, as in the real testbed measurements. In accordance with the testbed measurements

the input power is set to 23.5 dBm for every antenna. The placement of C-MIMO transmitters is shown in Fig. 3.6a. The transmitters for the D-MIMO system are placed at a height of 1.35 m along the two corridors. This is shown in Fig. 3.6b.

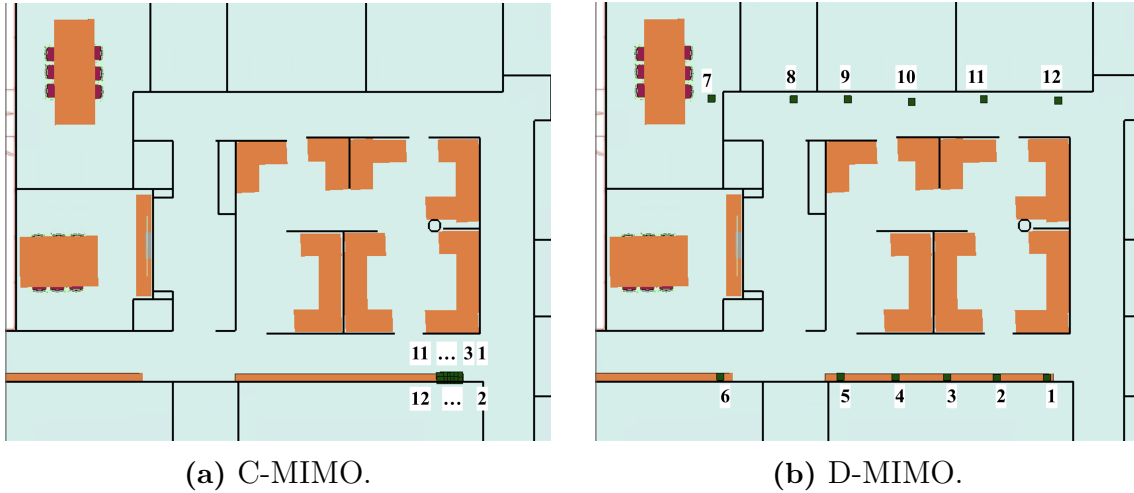


Figure 3.6: Images showing the placements of transmitters for both (a) C-MIMO and (b) D-MIMO in the indoor environment. The placement is according to their respective locations during the testbed measurements.

For the outdoor simulation, the C-MIMO antennas are placed together at a height of 1.9 m and 2 m above the ground. The placement of the C-MIMO transmitters is shown in Fig. 3.7a. The transmitters for the D-MIMO system are spread over the area at a height of 1.35 m above the ground, which is shown in Fig. 3.7b. In order to possibly conduct real measurements based on this simulation the reach of the testbed was taken into account when placing the D-MIMO transmitters. The antennas are connected to the CPU with fiber optic cables that are 30 m long, therefore the antennas were placed in a circle of approximately 60 m in diameter. Unlike the indoor simulations, the D-MIMO antennas are now directed in different directions, as can be seen by the directions of the arrows in Fig 3.7b.

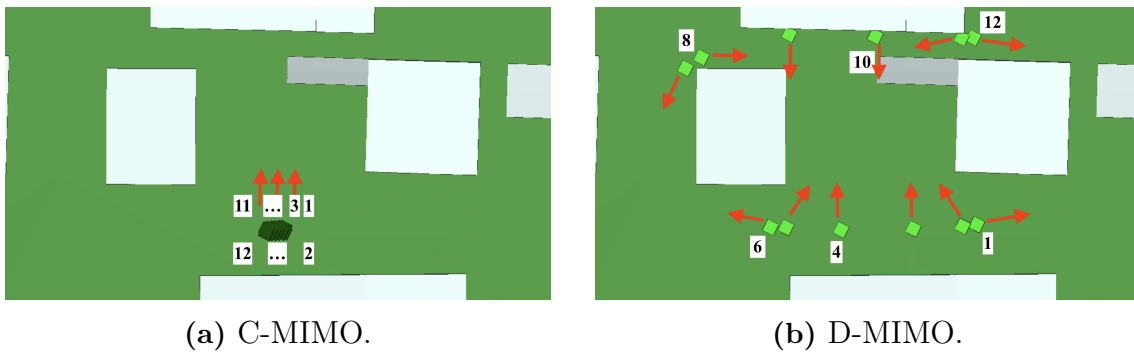


Figure 3.7: Images showing the placements of transmitters for both C-MIMO and D-MIMO for the outdoor simulation. The arrows in (b) indicate the directions of the antennas.

3.2.6 Receivers

In the same way as the transmitters; the receivers are placed in the floor plan and assigned an antenna. For the measurements, the receiver is placed on a robot that follows a trajectory around the office area as shown in Fig. 3.8a. The robot moves around the room in a counterclockwise direction and the 1–44 positions are referred to as shown in Fig. 3.8a. Instead of using a trajectory of receivers as in Fig. 3.8a a grid of receivers was constructed, which is shown in Fig. 3.8b. The height was set to 1.4 m to correspond with the height of the robot. By using a grid the signal strength of the entire area of interest can be measured, not only the trajectory. The points that are located on the path of the robot are isolated from the grid for comparison with the testbed measurements.

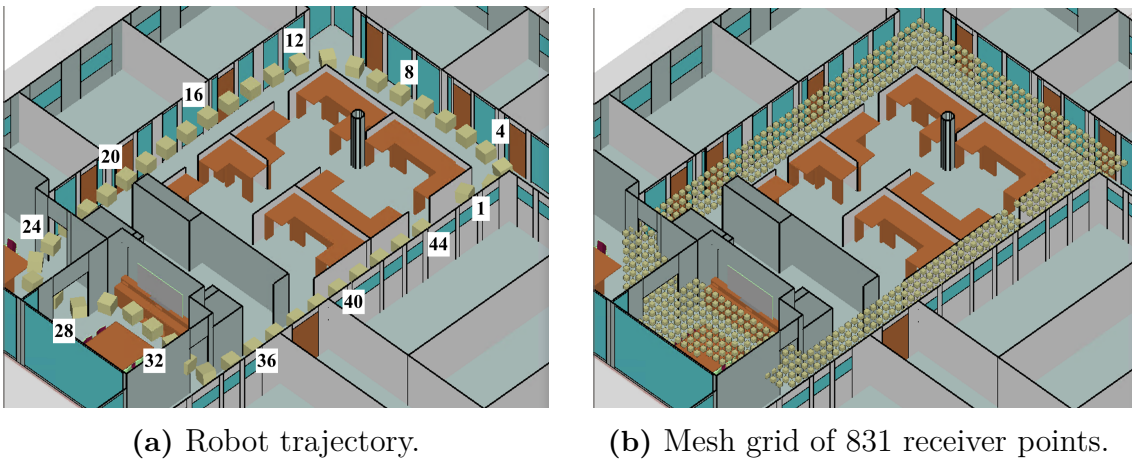


Figure 3.8: Images showing both (a) the robot trajectory during the measurements and (b) the grid of receiver points used in the simulation.

For the outdoor simulation the same method is used. Since there are no testbed measurements yet there is not a robot trajectory to simulate. However, in order to be able to recreate the simulations in future measurements a trajectory was made as can be seen in Fig. 3.9a. As described above a mesh grid of receivers was used at a height of 1.4 m from which points the corresponding to the trajectory are isolated. The mesh for the outdoor environment is shown in Fig. 3.9b.

All receivers are assigned the omnidirectional antenna and the receiver points are configured to not interfere with each other. The placement of transmitters and receivers is the last step of constructing the environment for simulation.

3.2.7 Study Area

After the simulation environment is built, the next step is to construct a study area. The study area specifies the bounds of the simulation. It defines the region of the simulation, the propagation model and the types of outputs desired.

The input parameters that can be changed to affect the simulation propagation

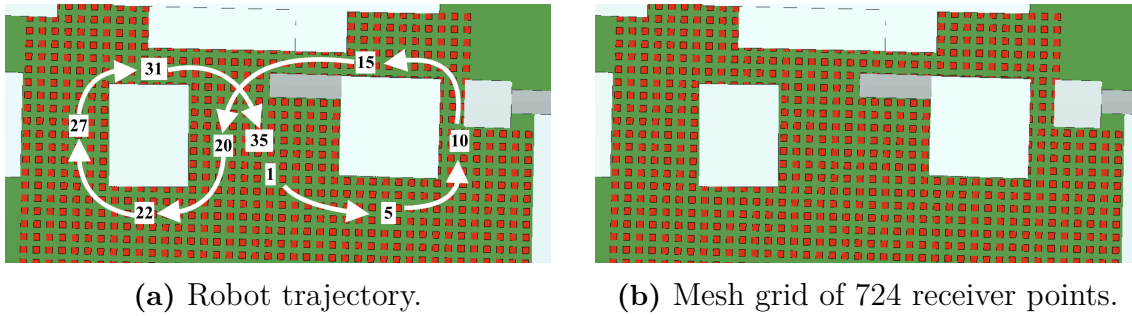


Figure 3.9: Images showing both (a) a possible trajectory for future measurements and (b) the grid of receiver points for the outdoor simulation.

models are ray spacing, number of reflections, -transmissions and -diffractions. The ray spacing specifies the angle between the transmitted rays. The number of reflections specifies how many reflections of each ray that will be taken into account during the simulations. The number of transmissions specifies how many dielectric materials every ray will transmit through. The number of diffractions determines how many times the rays will diffract, each diffraction will act as a new transmitter and therefore significantly increase the number of rays in the simulation. Increasing any of these parameters will result in a more precise model but also increase both the complexity of the simulation and the computational time. Parameters that will produce a sufficiently accurate model were chosen according to the reference manual and after comparing different combinations, these are presented in Table 3.3.

Table 3.3: Table showing the chosen input parameters for the study area for both the indoor and outdoor simulations.

Input parameter	Chosen parameter
Ray spacing	0.2°
Number of reflections	4
Number of transmissions	2
Number of diffractions	1

Different output parameters can also be chosen from the study area. For this project, the data collected from the study area will be used to create the simulated channel matrix. Therefore, the chosen output is the *Complex impulse response* since this is what is needed to calculate the capacity in accordance with (2.5). In order to create a map of received signal power, hereafter referred to as heat map, the output *Received power* was also included. This is used by the *communication systems* feature, as explained in Section 3.2.8, in order to illustrate a heat map.

3.2.8 Communication Systems

As shown in Fig. 3.2, Wireless InSite is divided into tabs and the second to last tab is called Communication systems. This is an additional feature/tool in Wireless InSite that uses the outputs from the study areas for additional post processing and

calculations. The communication systems can, for example, calculate bit error rate and interference. The calculation that is used in this project from the communication systems is the received power at every receiver point.

The output that is used in the communication systems results are from the analysis type called *Interference and Receiver Summary Files Only*. The output of interest is the received power at every receiver from the transmitters. This is used to construct a heat map of the received power in the entire environment and a figure showing the received power at each of the measurement points.

3.2.9 Output

The data from the study areas and communication systems is gathered as a tree structure in the output tab. If a study area is named, for example, *C-MIMO study area* this can be expanded and the requested outputs from the study area and the communication systems calculations are shown. In this way data can be illustrated in the project, such as heat maps, or the data can be exported to text files. An example of a text file containing the complex impulse response for a transmit antenna can be found in appendix A.

4

Indoor Environment

This chapter will present the results from the simulations for the indoor environment. Each result is presented in individual sections that first account for the method of how the results are calculated followed by the result itself. Sections 4.1.1–4.3.2 includes a comparison with the measurement data. After this a study of antenna removal is performed in order to investigate the effect on both C-MIMO and D-MIMO when different antennas are inactive. This will give an indication of the robustness of the systems. All sections represent a MU-MIMO DL scenario with 4 users with a SNR for the simulations of 27.5 dB.

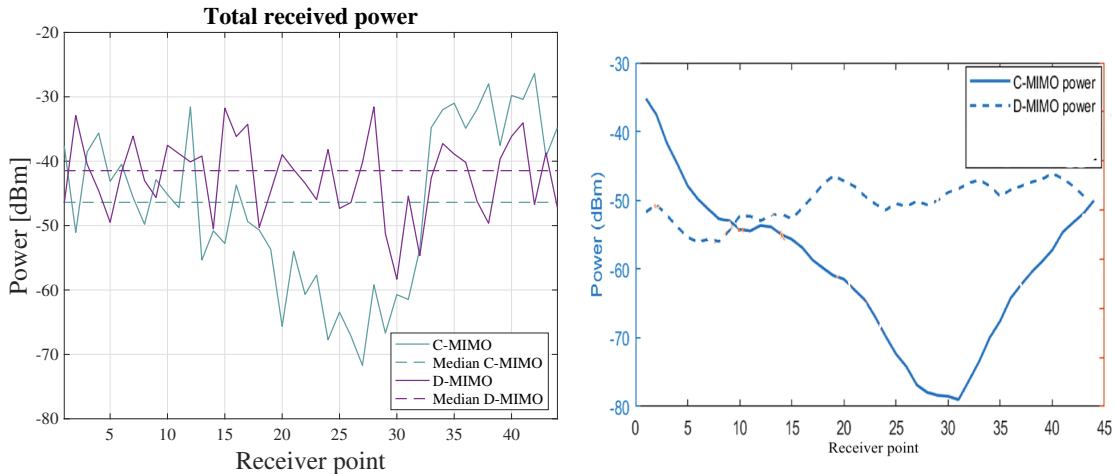
4.1 Received Power

The received power is found in the text file generated by the Communication System of Wireless InSite, as further explained in Section 3.2.8. This text file includes, amongst other things, received power and received power with phase for every receiver point in the grid. By extracting the receiver points in the simulation that correspond to locations of the measurements the received power can be compared. For the comparisons in this study the received power with phase is being presented. This means that the transmit antennas radio waves can interfere in a constructive or destructive manner.

4.1.1 Resulting Received Power for Each Receiver Point

The received power in each of the 44 receiver locations for C-MIMO and D-MIMO is depicted in Fig. 4.1. For C-MIMO the decrease in power can be seen between position 20 to 35 which are located in area A. The propagation path between area A's receiver points and the C-MIMO transmit antennas are blocked by concrete walls. Also, the received power is higher in the positions close to the C-MIMO antennas compared to D-MIMO antennas.

The received power shows what is expected from a C-MIMO and D-MIMO system. Since the antennas for D-MIMO are spread throughout the office area, the received power is more uniform for the whole area as shown in Fig. 4.1. For C-MIMO, all antennas are located at the same position, so for users that are located between position 20 to 35, found in area A, there is no LoS signal component. This creates



(a) Simulations.

(b) Measurements. From [16]. Adapted with permission.

Figure 4.1: Total received power at each receiver location from both C-MIMO and D-MIMO transmit antennas with center frequency of 2.365 GHz.

a reduction of received power.

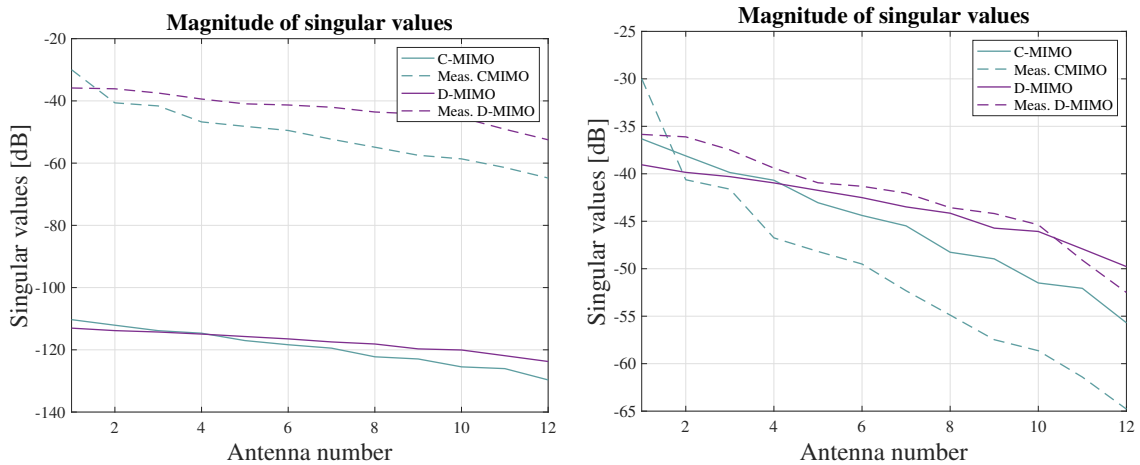
There are similarities between the results from the measurement, Fig 4.1b, and the simulations, Fig 4.1a. Both show the same trend, especially the power loss in area A. However, the magnitude of the received power is larger in the simulations. This could be due to unknown losses in the hardware equipment that is not a factor in the simulations and differences in a real environment and a model. Also, the received power to the points located in front of the C-MIMO antennas is larger in the measurements compared to the simulations. This can be due to antenna placements and the phase interfering in a more constructive way for the measurements. A figure illustrating the received power without phase taken into account can be found in Appendix B.1, which represents the received power without the phase interference.

4.2 Singular Value Spread

As stated in Section 2.2.1, the singular value spread is a measure of the variation in channel quality between different subchannels. To find the singular values the first step is to calculate the channel matrices, \mathbf{H} , for both the C-MIMO and D-MIMO system. This is done as in (2.5) described in Section 2.1.4. The channel matrices are of size 44×12 where the rows correspond to the 44 receiver points and the columns correspond to the 12 transmitter antennas.

Due to the equipment that was used performing the actual measurements there is a scaling factor of 5,000 applied to the simulated channel matrix. The reason is that the received signal for the measurements were collected in a universal software radio peripheral (USRP), which is seen as a black box. Therefore, it is unknown how the

signal is treated inside of it. The magnitude of the singular values before and after the scaling factor can be seen in Fig. 4.2a and 4.2b.



(a) Singular values before scaling factor. (b) Singular values after scaling factor.

Figure 4.2: Showing the difference in order of magnitudes of the singular values before and after the constant is multiplied. The x-axis refers to the subchannel from the different transmitter antennas. Note the change on the y-axis. (a) Singular values before multiplied with a constant factor. (b) Singular values after multiplying the channel matrix with a constant factor of 5,000.

The singular values are found by first generating a matrix with every combination of 4 users positioned along the 44 receiver positions by using the Matlab function `nchoosek`. This gives a matrix of size $135,751 \times 4$ consisting of every user combination possible with no repetition. This matrix consisting of all possible user combinations will be used in the following result Chapters, 5 and 6, and will hereafter be referred to as $User_{comb}$. The singular value spread is calculated as (2.11).

A new channel matrix of size 4×12 is created by isolating the 4 rows corresponding to the $User_{comb}$ user positions in the channel matrix. This step is repeated for both C-MIMO and D-MIMO. SVD is performed on these 4×12 matrices, as in (2.7), and the resulting singular values are saved. This way the singular value spread is calculated for every possible user combination with 4 users.

4.2.1 CDF of Singular Value Spread

The singular value spreads for C-MIMO and D-MIMO can be seen as a cumulative distribution function (CDF) in Fig. 4.3. The spread is calculated using (2.11) which means that a small value, far to the left in Fig. 4.3, indicates a large singular value spread. As seen in Fig. 4.3, the singular value spread for C-MIMO is larger than for D-MIMO. This means that the singular values have more variations in C-MIMO which means a larger variety of channel quality, as explained by (2.11). For D-MIMO, the singular values have less variety so the channel quality between the users are more alike than for C-MIMO. This is because there are more users that

experience LoS connections for D-MIMO. True for both C-MIMO and D-MIMO is that the measurements have a larger singular value spread compared to the simulations and therefore more variety in the channel quality. Worth mentioning is that this metric alone does not contain information about the channel quality, but only the variation in channel quality between the users.

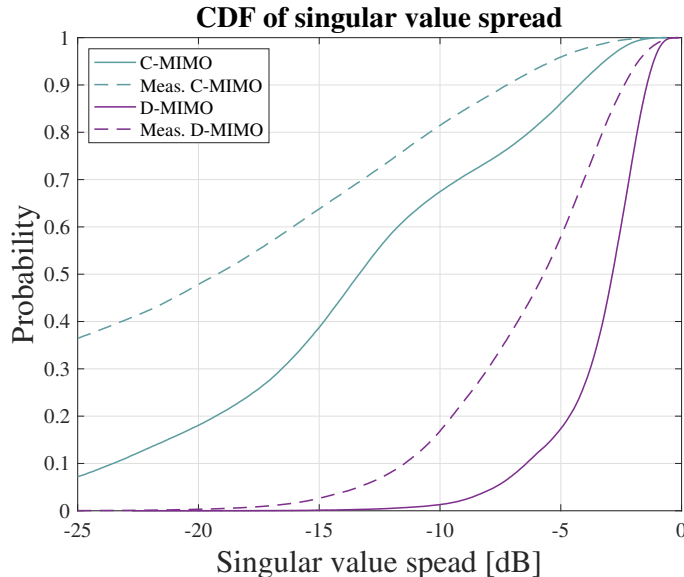


Figure 4.3: A CDF showing the singular value spread for C-MIMO and D-MIMO from both measurements and simulation. A small spread is close to 0 dB.

One reason for the difference in singular value spread between the measurements and the simulations could be that there are more losses in the real system. The simulation does not account for hardware losses, but simulates based on the parameters and settings that are given. Also, there are more obstacles and details in the real environment that is not included in the simulated model which could affect the singular value spreads.

4.3 Capacity

The capacities of the systems presented in this chapter are the user capacity, calculated as (2.15), and the sum capacity, calculated as (2.16). As seen in (2.15) and (2.16) the capacities are calculated using the singular values. These are found as explained in Section 4.2: every user combination is taken into account using the matrix \mathbf{User}_{comb} and SVD is performed on the 4×12 channel matrices to calculate the singular values. To calculate the capacities the SNR is set to 27.5 dB for the simulations and 35 dB for the measurements. The true SNR for the measurements is unknown, as explained in the associated paper [16], and was estimated for the following comparisons. The different SNRs are to match the simulated data of the D-MIMO system with the D-MIMO system for the measurements.

4.3.1 User Capacity per Position

In Fig. 4.4 the user capacity for each of the 44 positions are shown in a box plot. Noteworthy is how the capacity can differ for a user at one of the 44 positions. This difference for a position changes depending on what other users/positions operate on the channel at the same time. Every position is represented with a blue box where the top and bottom of the box represents 75th and the 25th percentiles of the capacity, respectively. The red line is the median capacity and the dashed tails extends to the maximum and minimum capacity, not including outliers.

Fig. 4.4a shows that the D-MIMO system provides a more stable capacity regardless of the position shown with the smaller boxes. The user capacity for C-MIMO shows a larger variation and is hence more dependent on the positions of the other users. It can also be seen that the median drops significantly for C-MIMO for the positions in area A, positions 20–33.

When comparing the simulations to the measured data the user capacity for D-MIMO is similar. In both Fig. 4.4a and Fig. 4.4b, the D-MIMO systems have roughly the same median and although the variation is somewhat smaller for the simulations they are still in the same order of magnitude. For C-MIMO, it can be seen that the overall magnitude is larger for the simulations as compared to the measurements. The simulations also have a larger variation across all positions while the measurements show a clear increase in variation in the positions close to the transmitter antennas.

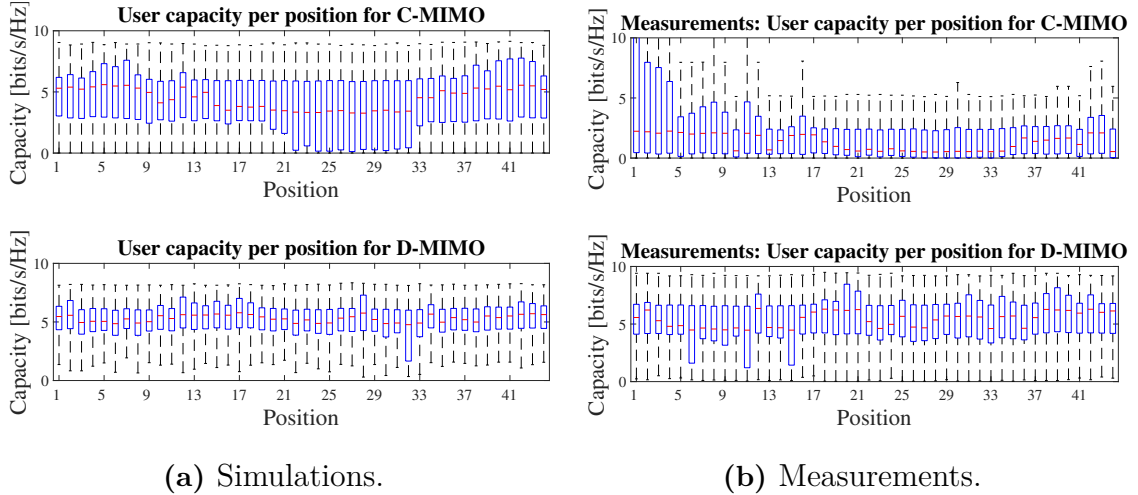


Figure 4.4: Boxplot showing the user capacity for each location containing all 135,751 combinations in the case of 4 users being placed at the 44 positions.

As can be seen in Fig. 4.4, the user capacity per position for C-MIMO has a larger variation compared to D-MIMO. This is because the user’s capacities also depend on the remaining users of the system. In a C-MIMO situation where one user is optimally located near the 12 antennas; if the remaining users are all located in area A, the capacity of the first user will be negatively affected by this. Mathematically,

this is due to the nature of SVD. This can explain the larger variation of the boxes for C-MIMO.

4.3.2 Histogram of the Sum Capacity

The sum capacities for C-MIMO and D-MIMO are plotted as a histogram in Fig. 4.5. In Fig. 4.5a, it can be seen that D-MIMO has a higher mean value of the sum capacity and never has a sum capacity lower than 10 bits/s/Hz. The sum capacity for C-MIMO has a higher variation compared to D-MIMO and a lower mean value. It can be noted that the sum capacity for D-MIMO is more concentrated close to the maximum value compared to C-MIMO since the variation is smaller for D-MIMO.

When comparing the simulated data, Fig 4.5a, to the measured data, Fig 4.5b, it can be seen that there are some differences. For D-MIMO there is a larger variation of the capacity for the measured data. There is also a larger difference in performance between C-MIMO and D-MIMO in the measured data. The SNR is adjusted in the simulations in order to align the mean values of the D-MIMO capacities. With a similar mean between the D-MIMO systems the mean for the C-MIMO system is significantly lower in the measurements compared to the simulated C-MIMO. Figures showing the sum capacity with different SNR values for the simulations can be found in Appendix B.2.

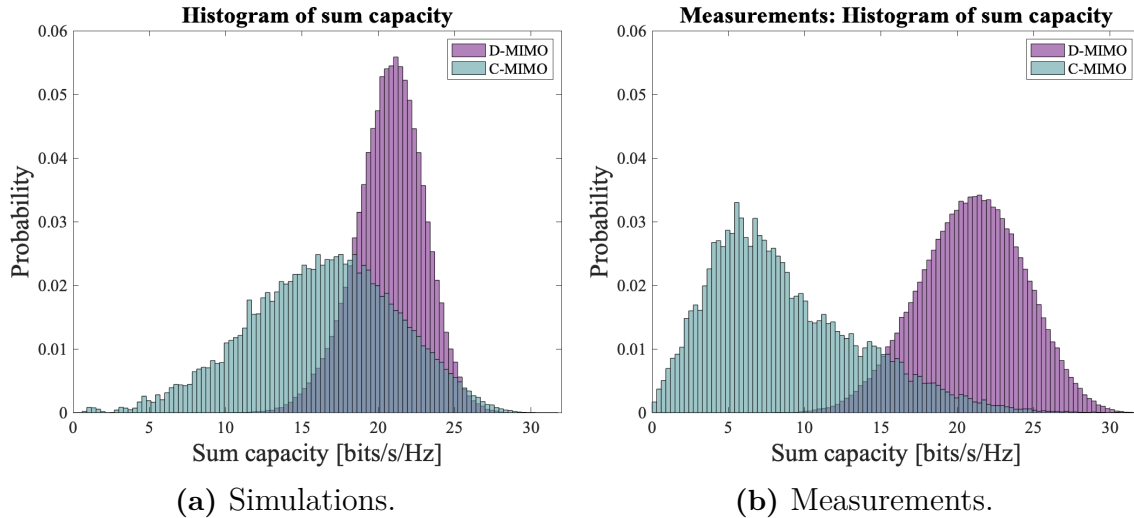


Figure 4.5: Histogram showing the sum capacities for C-MIMO and D-MIMO.

The sum capacity is a metric that includes every user in the MIMO system, so even if a single user has exceptional capacity the sum capacity can still be small if the remaining users experience bad capacity. The comparison in Fig. 4.5 shows that D-MIMO has overall higher sum capacity compared to C-MIMO. This is a result of the fact that the subchannels can be considered to be more independent when spatially separated. Another factor is that C-MIMO systems are more affected by shadowing and therefore experience a greater difference in quality for the user depending on the location.

4.4 Antenna Removal

This study consists of investigating the effect of removing transmitter antennas for both C-MIMO and D-MIMO in an indoor environment. The purpose is to analyse the effect on the sum capacity of each system with different number of antennas.

First, the sum capacities for all user positions, \mathbf{User}_{comb} , must be calculated for all antenna combinations ranging for all 12 antennas down to using only 4 antennas. All possible antenna combinations are generated in the same way as \mathbf{User}_{comb} , accounted for in Section 4.2. The number of possible antenna combinations differs depending on the number of antennas. The number of combinations are shown in Table 4.1.

Table 4.1: The different number of possible antenna combinations when using different number of active antennas.

Number of antennas	Combinations
12	1
11	12
10	66
9	220
8	495
7	792
6	924
5	792
4	495
Total	3,797

By calculating the sum capacity for all combinations of users and antennas, the result is a $3,797 \times 135,751$ matrix consisting of every sum capacity for every combination. Then, to investigate which antennas that are important to maintain high capacity the following procedure is followed. The $3,797 \times 135,751$ matrix is averaged over each antenna configuration for the sum capacities which creates a $3,797 \times 1$ vector containing the average sum capacity of every user combination per antenna combination. Now, this vector can be used to compare the average sum capacity over all user placements for each antenna combination. This is done for both C-MIMO and D-MIMO yielding two $3,797 \times 1$ matrices.

4.4.1 Sum Capacity for Each Antenna Combination

Fig. 4.6 shows the average sum capacity of every combination of 4 users for every antenna configuration. The dashed lines illustrate the removal of one antenna, i.e. between two dashed lines are the same number of antennas but there are different antenna combinations. The removal starts with removing one antenna, then two, and so forth, until 8 antennas are removed. The most number of possible antenna combinations are when 6 antennas are removed as shown in Table 4.1. The y-axis shows the averaged total sum capacity of all user combinations. That is, for

antenna combination N_{comb} the sum capacity for all user combinations is calculated and averaged. The darker lines illustrate the mean in each interval. Fig. 4.6b is a close up of Fig. 4.6a showing the first 350 antenna configuration's average sum capacities. The number of antenna combinations is smaller when only removing one or two antennas, the close up provides a clearer visualisation of this narrow range.

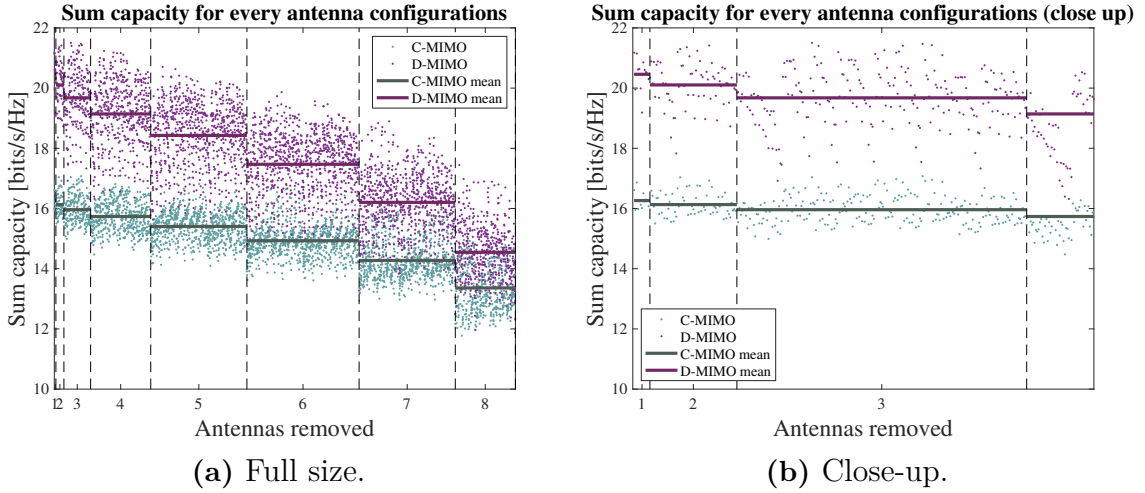


Figure 4.6: Graph showing the average sum capacity for all user and antenna combinations for both C-MIMO and D-MIMO. The x-axis is all different antenna combinations with a decreasing number of antennas. Change in number of removed antennas is represented by the dashed lines.

The size of each interval is dependent on the number of combinations, presented in Table 4.1. The y-axis is the average of the total sum capacity for all user combinations. The darker lines show the mean in each interval.

(a) Average sum capacity for all user combinations versus every antenna configuration. (b) Showing the same as Fig. 4.6a but zoomed in to show the first 350 antenna combinations.

The same data shown in Fig. 4.6 is illustrated in a different manner in Fig. 4.7. Every sum capacity for a set number of removed antennas is represented with a blue box where the top and bottom of the box represents 75th and the 25th percentiles of the capacity, respectively. The red line is the median capacity and the dashed tails extend to the maximum and minimum capacity, not including outliers. In short, a box in Fig. 4.7 shows the same data as what is shown between two dashed lines in Fig. 4.6.

From Fig. 4.6a it can be seen that D-MIMO has overall a larger capacity than C-MIMO. This means that to achieve a given sum capacity more antennas can be removed for D-MIMO than C-MIMO.

By studying the sum capacity for all combinations of users and antennas, shown in Fig. 4.6 and Fig. 4.7, the sensitivity of the two systems can be observed. From Fig. 4.6 it can be seen that for both C-MIMO and D-MIMO the sum capacity varies depending on which antenna that is removed. The larger fluctuations for D-MIMO is a result from the spatial diversity in the system; the distribution of antennas

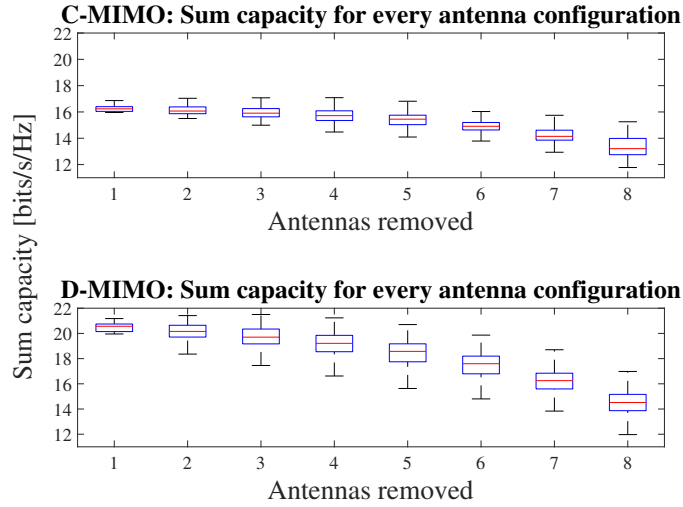


Figure 4.7: Boxplot showing the average sum capacity for all user and antenna combinations for both C-MIMO and D-MIMO. The x-axis shows the number of antennas removed. The y-axis is the average of the total sum capacity for all user combinations with the red line being the median.

provides better overall coverage but also makes the system less robust when it comes to removing antennas. The sum capacity for D-MIMO is more dependent on which antenna that is removed. As previously stated in Section 4.1.1, D-MIMO provides a more uniform coverage compared to C-MIMO. But if, for example, the antennas removed are located in area A, it will affect D-MIMO’s antenna distribution and the overall capacity will decrease. The variation is smaller for C-MIMO since the antennas are located closer together, and is therefore less dependent on the specific antenna removed.

The variation in average sum capacity when removing different antennas, shown as the fluctuations of C-MIMO and D-MIMO in Fig. 4.6, is the result of a constructive and destructive effect when combining the complex impulse responses to create the channel matrices. Since the propagation data includes both magnitude and phase, the rays could amplify or cancel each other depending on the incoming signals at the receiver points. However, the mean values in Fig. 4.6a indicates the overall capacity trends when removing antennas. For both systems the trend is a decrease in capacity when removing antennas which is what is expected since the received power of the incoming signals would be less. It can be seen that C-MIMO has a smaller decline in sum capacity. This means that the system is less sensitive in terms of removing antennas compared to using all 12 antennas. However, while C-MIMO is less affected by removal of antennas, D-MIMO still provides a larger average sum capacity.

4.4.2 Capacity Decrease From Removal of Antennas

This section will examine the capacity decrease for C-MIMO and D-MIMO when removing different number of antennas. In order to compare the systems in regards to removing antennas a reference capacity was used. The following comparisons will be made in reference to 95% of the C-MIMO system when using 12 antennas, which in this case is 13.3898 bits/s/Hz. The 3, 797 \times 1 matrices with sum capacities for C-MIMO and D-MIMO, as explained in Section 4.4, are used here to compare with the 95% reference capacity. The results are found in a boxplot in Fig. 4.8. Each number of removed antennas is represented with a blue box where the top and bottom of the box represents 75th and the 25th percentiles of the capacity, respectively. The red line is the median capacity and the dashed tails extends to the maximum and minimum capacity, not including outliers.

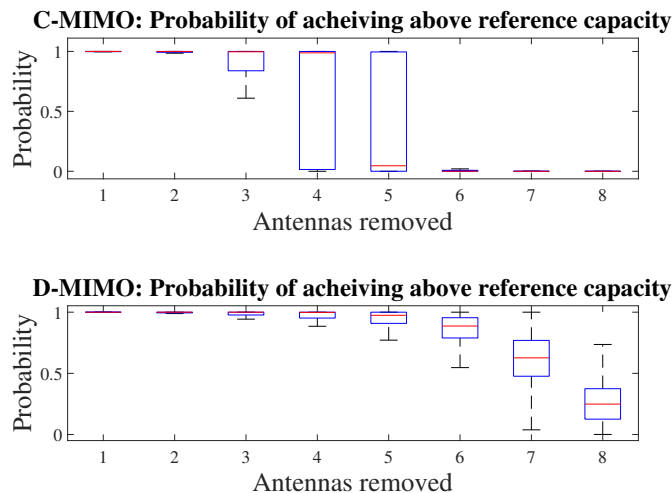


Figure 4.8: Boxplot showing the probability of a C-MIMO system and D-MIMO system to achieve a reference capacity with different number of antennas removed. The x-axis shows the number of antennas removed and the y-axis is the probability with the red line being the median.

From Fig. 4.8 it is clear that D-MIMO in many cases can achieve a higher capacity than C-MIMO. After removing 5 antennas the C-MIMO system almost never reaches the reference capacity of 95% when using 12 antennas for C-MIMO. D-MIMO can for most cases reach the reference capacity with 7 antennas removed. Even in the case with 8 antennas removed, D-MIMO can still achieve the reference capacity while this is never the case for C-MIMO.

4.4.3 Antennas Present When Achieving Above Average Sum Capacity

The antenna configurations that provide an above average sum capacity for the D-MIMO system are identified and Fig. 4.9 shows the occurrence of each antenna amongst these combinations. Each box represents 1 of the 12 antennas. In each of

the 8 removal intervals, represented as dashed lines in Fig. 4.6, the configurations that provide a sum capacity above the average sum capacity is isolated. The isolated configurations are the dots illustrated above the thick line in Fig. 4.6. In each interval the occurrence of each individual antenna is calculated. The occurrence is given in percent: out of the configurations providing the above average capacity, it shows in how many of these a specific antenna appear. This will show the most significant antennas in the D-MIMO system. The placements of the antennas can be seen in Fig. 3.6b.

From Fig. 4.9 it can be seen that the most significant antennas are 6, 7 and 11. Antennas number 6 and 7 are located in area A. The appearance of at least one of them will provide coverage in this, otherwise isolated, area. Antenna 11 is located in the corridor close to a corner. A possible explanation for this antenna's significance could be that it covers the corridor not housing any transmitters at same time as it provides coverage for the rest of the room better than antenna 12. However, this theory is a theory that has not been confirmed and could require further study.

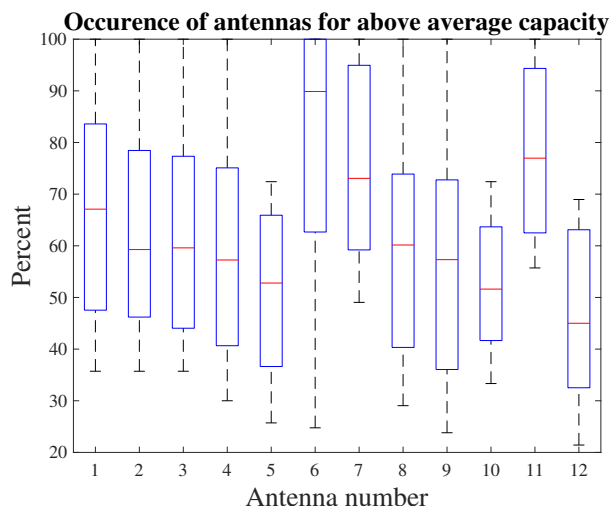


Figure 4.9: Boxplot of the occurrence of each antenna in the configurations that provide an above average sum capacity in the D-MIMO system in percent. Each box represents the occurrence in percent of one specific antenna in the above average antenna configurations.

4.5 Discussion

The first step of this indoor study was to achieve a simulation environment that could represent the real measurements. The results from the simulation is compared to the results from the measurements and they both show similar trends. In both cases there is a decrease in received power and capacity when users are located in area A. The overall sum capacity for D-MIMO compared to C-MIMO is better and has less variation, meaning it is a more stable system.

A noticeable difference between measurements and simulations is that the C-MIMO

system in the simulations performed better than in real life. This is most noticeable in the box plot for user capacity, Fig. 4.4, and the histogram for the sum capacity, Fig. 4.5. In the latter figure the capacity of the C-MIMO system has a mean closer to D-MIMO in the simulations than in the measurements. This could not be mitigated by varying the SNR, which affected both D-MIMO and C-MIMO equally and hence did not separate them further as desired. The SNR for these results was set by aligning the mean of the D-MIMO capacities.

The study concerning antenna removal shows that the D-MIMO system provides better or equal capacity to the users with a significantly smaller number of antennas. When comparing to the number of antennas needed to provide 95% of the C-MIMO capacity when using all 12 antennas, the D-MIMO system can deliver a stable performance with 6 to 7 active antennas while C-MIMO needs 8 or 9. The performance of the D-MIMO system varies depending on which antennas that are removed. The most common factor between the combinations providing the best capacity is that they include at least one antenna in area A. Hence, an antenna in the area most affected by shadowing is an important factor when considering antenna placement.

Building the model of the office area was an iterative process, meaning continuous improvements were made until achieving the results presented in this chapter. However, some settings remained constant during the process and no analysis was made to study the effect of these settings. This includes parameters such as materials and transmitter and receiver locations. No further studies regarding the parameter settings were made since the materials were specified according to ITU recommendation. What could be done was double checking the materials in every wall and also trying to more accurately mimic the environment in terms of wall thicknesses etc. Many details were excluded due to the amount of time it would require to include everything, for example: computers in area B, chairs in area B, furniture in the offices not surrounding the testbed, kitchen appliances in area A, to name a few. A study of the effect of these parameters could have improved the accuracy of the results in this chapter but also for Chapters 5 and 6.

The number of users in this study is constant: there are 4 active users. The choice of this specific number was initially based on the fact that there were 4 active users in the results for the measurements and in order to compare results this was not a factor that was changed. Later in the project, there were discussions concerning changing the number of users and some experiments were made in Matlab. The change in number of users did however not affect the results significantly, and it was therefore kept for the upcoming results in the project as well.

Future work in the indoor study would mainly be to use this simulation method in other indoor environments.

5

Frequency Comparison

This study consists of comparing the results using two different center frequencies in the same indoor model. This will act as an initial study of the implementation of using mmWave frequencies in this system. The frequencies are 2.365 GHz and 28 GHz. The results from 2.365 GHz are the same as in Chapter 4. This chapter will compare results of the two frequencies divided into received power, singular value spread, sum capacity and user capacity per position.

5.1 Received Power

The received power of each simulation is gathered from the communication system function in InSite as explained in Section 3.2.8. Wireless InSite calculated the resulting received power in each receiver point from each ray in the simulation. As stated in Section 3.2.4, for the 28 GHz simulation the antennas used are omnidirectional antennas with default settings.

5.1.1 Comparison Between the Received Power

Heat maps of the received power for frequencies 2.365 GHz and 28 GHz in the office area can be seen in Fig. 5.1 for C-MIMO and in Fig. 5.2 for D-MIMO. The range for both C-MIMO and D-MIMO is between -80 dBm (purple) to -30 dBm (red).

In Fig. 5.1 and 5.2 it is seen that both systems are affected in a similar way. The received power is more affected by shadowing when using 28 GHz compared to 2.365 GHz. Both for C-MIMO and D-MIMO, there is a decrease in power in area A. It can be seen in Fig. 5.2 that coverage of D-MIMO is not as uniform when increasing the power. The power is strongest along the corridors, close to the transmitter antennas. This is an effect of the decrease in range of a high frequency signal.

The received power in each of the 44 receiver locations is depicted in Fig. 5.3 for both 2.365 GHz and 28 GHz. Similar to 2.365 GHz, the power drops significantly for C-MIMO in area A when using 28 GHz, Fig. 5.3b. In Fig. 5.3b it can be seen that there is a decrease in power in area A for D-MIMO as well, which is not as present in Fig. 5.3a. This could be due to the fact that the lower frequencies have a better ability to penetrate obstacles, such as walls, which surround this specific area.

Therefore the effect of shadowing is more noticeable when increasing the frequency. Low frequency signals also preserve their signal strength over distances better than high frequency signals.

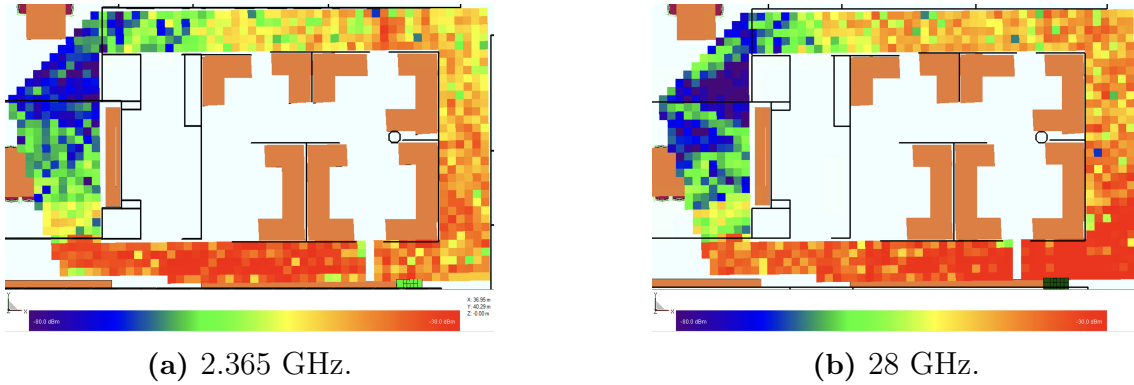


Figure 5.1: Heat maps over the office area for C-MIMO using a center frequency of 2.365 GHz and 28 GHz.

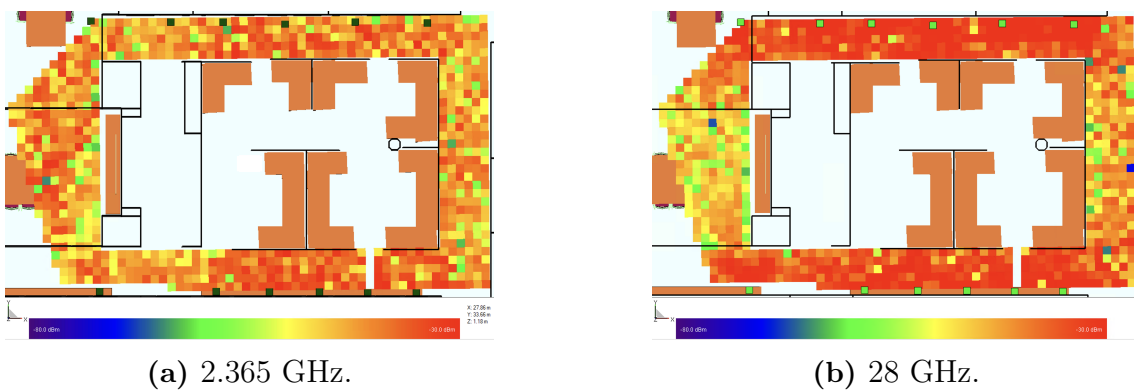


Figure 5.2: Heat maps over the office area for D-MIMO using a center frequency of 2.365 GHz and 28 GHz.

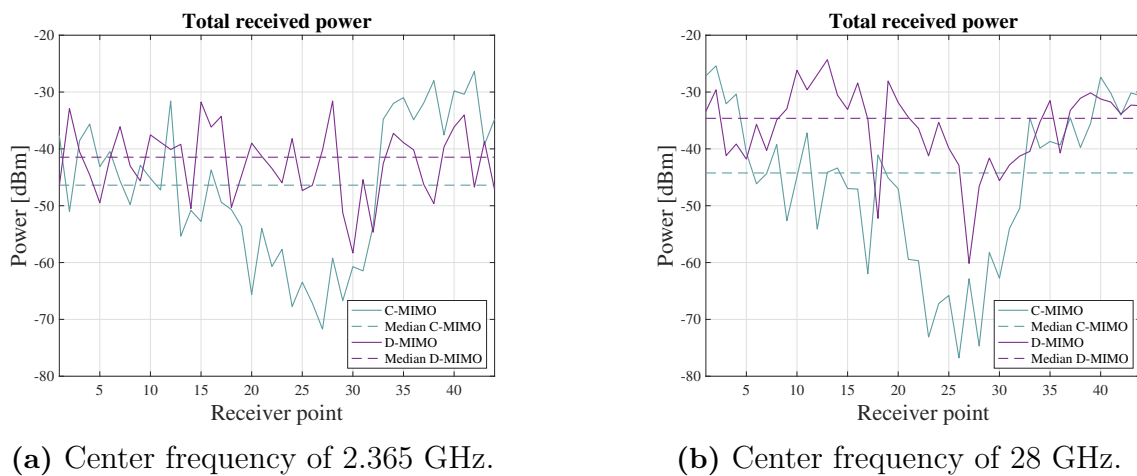


Figure 5.3: Total received power for each receiver point. The dashed lines illustrate the median of the received power calculated in Watts.

5.2 Singular Value Spread

For both 2.365 GHz and 28 GHz the singular value spread is calculated with (2.11). The singular values used are generated by SVD of a 4×12 channel matrix. The 4 rows are the rows in the full channel matrix corresponding to the 4 active users. This generates 4 singular values that are used in (2.11) for calculating the spread. This is done for all possible user combinations among the 44 receiver points.

5.2.1 Distribution of Singular Value Spread

The distribution of the singular value spread is depicted in Fig. 5.4 for both 2.365 GHz and 28 GHz. The results show that the singular value spread increases when using 28 GHz. With a higher frequency the signal is more susceptible to obstacles and the larger spread is mainly a result of the decreased coverage in area A.

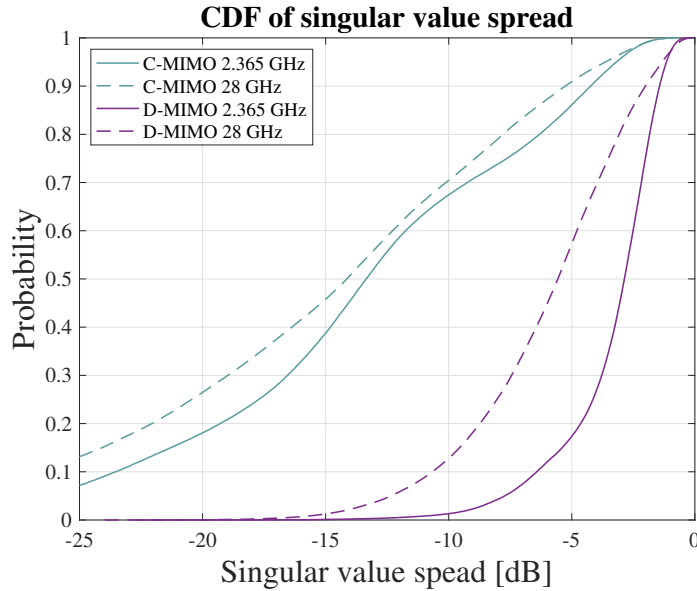


Figure 5.4: A CDF showing the distribution of singular value spread for C-MIMO and D-MIMO for both 2.365 GHz and 28 GHz. The singular value spread is calculated for all possible user combinations among the 44 receiver points. A small spread is close to 0 dB.

5.3 Capacity

The user- and sum capacity is calculated as described in Section 4.3 using (2.15) and (2.16). The following results correspond to a SNR of 27.5 dB.

5.3.1 User Capacity per Position

A box plot of the user capacity for each position is shown in Fig. 5.5. From this comparison it can be seen the variance of D-MIMO for 28 GHz has increased

compared to using the 2.365 GHz frequency. The effect of being located in area A (position 20 to 35) is visible with the increase in variance in this particular interval. There has also been an overall decrease in the mean of the user capacity for both D-MIMO and C-MIMO.

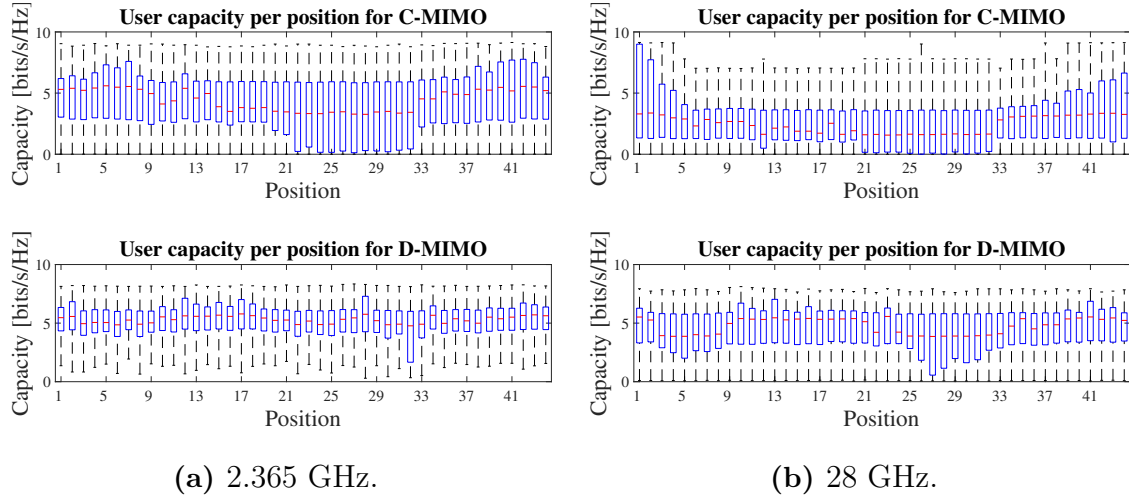


Figure 5.5: Boxplot showing the user capacity for each location in the case of 4 active users. Every position is represented with a blue box where the top and bottom of the box represents 75th and the 25th percentiles of the capacity, respectively. The red line is the median capacity and the dashed tails extends to the maximum and minimum capacity, not including outliers.

5.3.2 Histogram of Sum Capacity

The distributions of sum capacities for 2.365 GHz and 28 GHz are shown as histograms in Fig. 5.6. D-MIMO still has a larger mean than C-MIMO but when comparing Fig. 5.6a and 5.6b it can be seen that D-MIMO is more affected when increasing the frequency. The mean is reduced and the variance is increased. This indicates that there is a larger spread in channel quality due to the increasing shadowing in area A. The mean for C-MIMO is reduced when the frequency is increased.

5.4 Discussion

The results for the frequency comparison indicated that when increasing the frequency the two systems act more alike, more specifically D-MIMO starts to act more like C-MIMO. Shorter wavelengths reduce the signal's ability to penetrate objects as well as the propagation range. However, with the above stated effects of a high frequency signal the power is more concentrated, thus a reduction in capacity is present. The reduction is larger for C-MIMO compared to D-MIMO since one strength of a D-MIMO system is the ability to provide a more sufficient coverage.

When increasing the frequency most settings in Wireless InSite were changed. Due to a combination of lack of time and lack of easily available documentation, the change

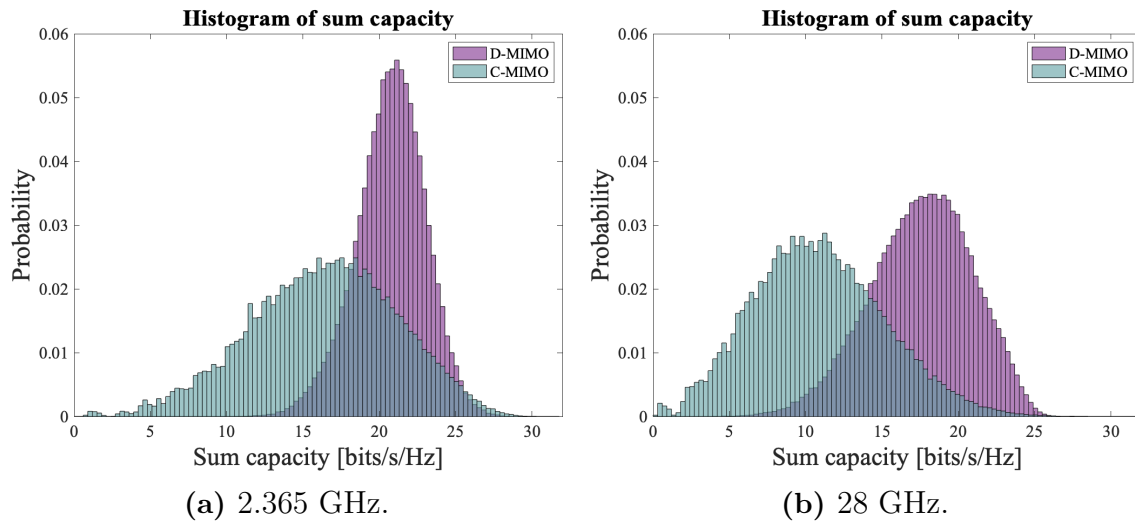


Figure 5.6: Histogram with the sum capacity calculated for all possible user combinations for (a) 2.365 GHz and (b) 28 GHz.

of settings could not be fully investigated. Factors such as what would happen to the waveform and antennas in a mmWave frequency system were overlooked. All antennas operating in the mmWave frequency simulation were set to default omnidirectional antennas and the waveform's only change compared to 2.365 GHz was the center frequency. Due to factors such as these, this study should be seen as an initial study of how this system would behave in the mmWave regime. It should be seen as a way to show what trends that could appear without emphasis on specific values of the results. More detailed and thorough simulations are needed. However, the materials used in the simulations were changed to 28 GHz specific materials, per ITU recommendations.

Future work for this study would be to further configure the simulated environment to a mmWave scenario.

6

Outdoor

This study consist of simulating C-MIMO and D-MIMO in an outdoor environment using a frequency of 2.365 GHz. The chosen environment is a pedestrian area located at Chalmers, with coordinates $57^{\circ}41'32.2''\text{N}$ $11^{\circ}58'31.6''\text{E}$. The environment was chosen due to the fact that it is located in between buildings in order to study the shadowing effect. A contributing factor is that the on-campus location would facilitate the possibility of conducting future measurements. This chapter will present the results gathered when simulating the systems on this location. The results are presented in individual sections, including received power, singular value spread and capacity performance. The sections will present both the method and the results of the study. The chapter ends with a discussion concerning this outdoor simulation.

6.1 Received Power

The received power is found in the text file generated by the Communication System of Wireless InSite, as further explained in Section 3.2.8. This text file includes, amongst other things, received power and received power with phase for every receiver point in the grid. By extracting the receiver points in the simulations that correspond to locations of the measurements the received power can be compared. For the comparisons in this study the received power with phase is being presented.

6.1.1 Heatmap of Power and Received Power per Position

In Fig. 6.1 a heatmap of the received power is presented. In the bottom of each figure is a scale and the range is between -120 dBm (purple) to -45 dBm (red).

The received power at each of the 44 receiver points is shown in Fig. 6.2. As can be seen both from this figure and in Fig. 6.1, both systems are affected by the shadowing of the buildings. The blue/green area in Fig 6.1a corresponds to receiver points 9–16 and 24–31 in Fig 6.2.

From Fig. 6.1b it can be seen that the D-MIMO system can provide better coverage behind the buildings compared to C-MIMO. In Fig. 6.2 the areas behind the buildings can be noted, but not as significantly as for C-MIMO. The difference in median illustrate this. The fact that the D-MIMO antennas were directed in different di-

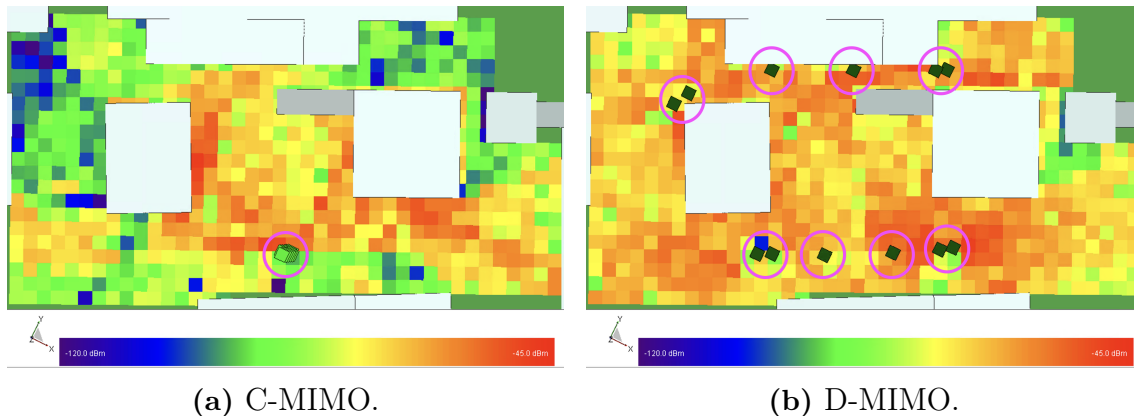


Figure 6.1: Heat maps of the outdoor environment for both C-MIMO and D-MIMO when using a center frequency of 2.365 GHz. The antenna positions can be found in the pink circles. The range is between -120 dBm (purple) to -45 dBm (red).

rections, illustrated in Fig. 3.7b, is a contributing factor to the coverage.

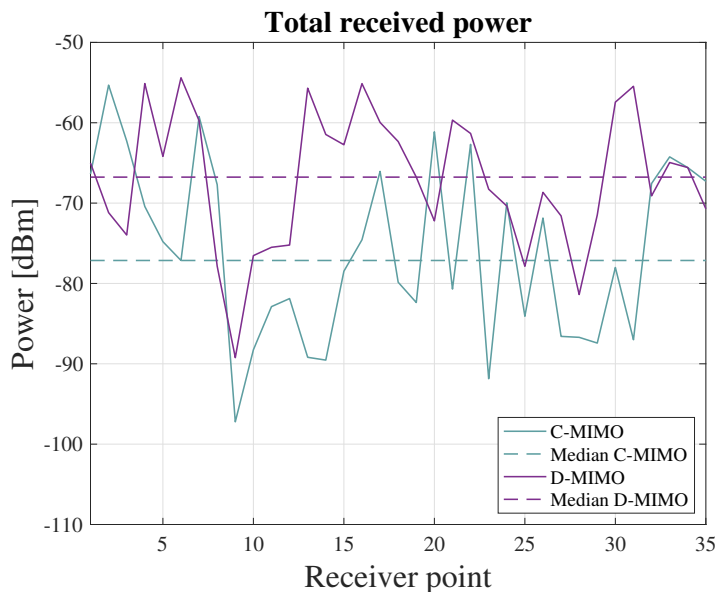


Figure 6.2: Total received power at each receiver location from both C-MIMO and D-MIMO transmit antennas with center frequency of 2.36 GHz from the outdoor simulation.

6.2 Singular Value Spread

The singular value spread is calculated with (2.11). The singular values used are calculated by SVD of a 4×12 channel matrix. The 4 rows are the rows in the full channel matrix corresponding to the 4 active users. This generates 4 singular values that are used in (2.11) for calculating the spread. This is done for all possible user combinations among the 35 receiver points. The matrix with all possible receiver

points is referred to as $User_{comb}$ and created as described in Section 4.2. However, the outdoor simulation contains 35 receiver points so the dimensions are now $52,360 \times 4$.

6.2.1 CDF of Singular Value Spread

The singular value spreads for C-MIMO and D-MIMO can be seen as a CDF in Fig. 6.3. The spread is calculated using (2.11) which means that a smaller value indicates a larger singular value spread. The singular value spread for C-MIMO is larger than for D-MIMO. This means that the singular values have more variations for C-MIMO which means a larger variety of channel quality. For D-MIMO the singular values have less variety so the channel quality between the users are more alike than for C-MIMO. This is because the subchannels are more independent with a larger spatial spread of the transmitters. There are also more users that experience LoS connections for D-MIMO. Worth mentioning is that this measure alone does not contain information about the channel quality, but only the variation in channel quality between the users.

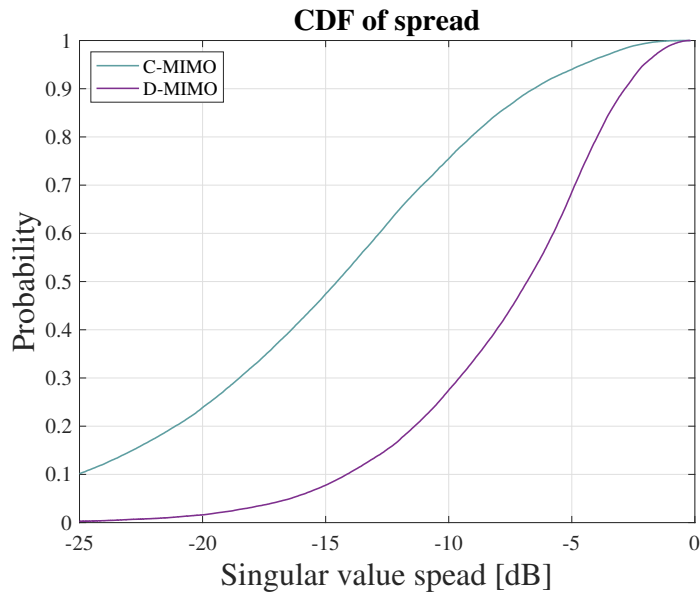


Figure 6.3: A CDF showing the singular value spread for C-MIMO and D-MIMO from the outdoor simulation. A small spread is close to 0 dB.

6.3 User Capacity

The user capacity for each individual user in a set of 4 is calculated using (2.15). This is repeated for all possible user combinations among the 35 receiver points, by iterating over each row in the matrix $User_{comb}$.

6.3.1 User Capacity per Position

A boxplot of the user capacity for each position is shown in Fig. 6.4. The capacity decreases in the receiver positions behind the buildings (receiver points 9–16 and 24–31) where shadowing occurs. This pattern could also be seen in Fig. 6.2. The effect of shadowing is most visible for C-MIMO (top in Fig. 6.4) where the median drops significantly at the affected positions. For D-MIMO (bottom in Fig. 6.4) the median only slightly decreases behind the buildings (receiver points 9–16 and 24–31) but the shadowing effect is visible when looking at the bottom of the boxes. This means that a larger portion of users experience a lower capacity in these regions than in the areas not affected by shadowing. The overall variance in D-MIMO is lower than for C-MIMO, which leads to a more uniform coverage.

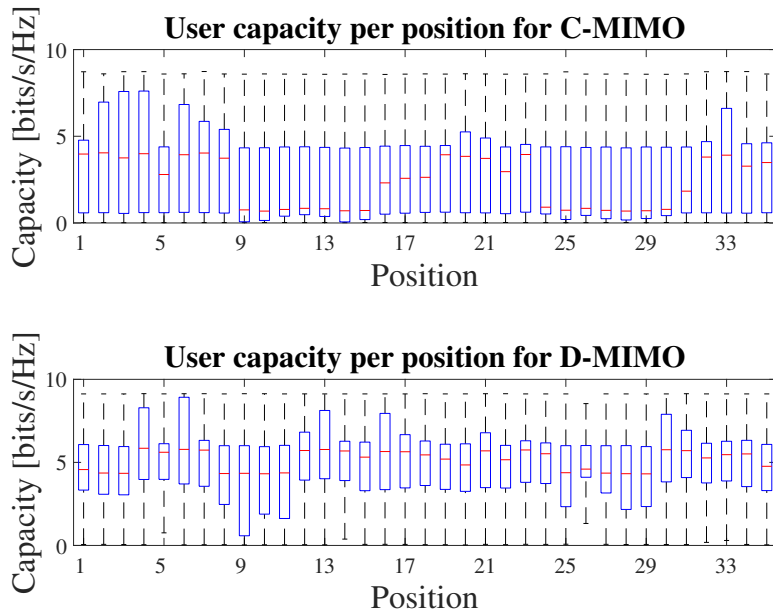


Figure 6.4: Boxplot showing the user capacity for each location in the case of 4 users in an outdoor environment.

6.4 Sum Capacity

The sum capacity is calculated using (2.16). For a given combination of 4 users the sum capacity is calculated, and this is repeated for all possible user combinations among the 35 receiver points, by iterating over each row in the matrix $User_{comb}$.

6.4.1 Histogram of the Sum Capacity

The distributions of sum capacities for C-MIMO and D-MIMO in the outdoor simulation are shown as a histogram in Fig. 6.5. It can be seen that D-MIMO has a higher mean value of the sum capacity and never has a sum capacity lower than 5

bits/s/Hz. The sum capacity for C-MIMO has a slightly higher variation compared to D-MIMO and a lower mean value.

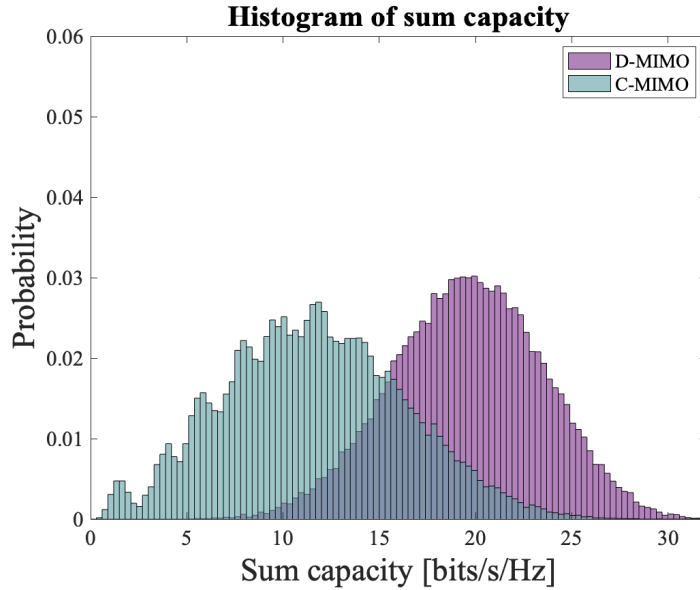


Figure 6.5: Histogram showing the sum capacities for C-MIMO and D-MIMO in the outdoor simulation.

The sum capacity is a measurement that includes every user in the MIMO system, so even if a single user has exceptional capacity the sum capacity can still be small if the remaining users experience bad capacity. The comparison in Fig. 6.5 shows that C-MIMO has overall less sum capacity compared to D-MIMO. This is a result of the fact that the subchannels for D-MIMO can be considered to be more independent when spatially separated. Another factor is that the C-MIMO system is being more affected by shadowing and therefore experiences a greater difference in quality for the user depending on the location.

6.5 Antenna Removal

The sum capacity for all possible combination of receiver positions and antenna combinations was calculated as described in Section 4.4

6.5.1 Sum Capacity All Combinations of Antenna- and User Combinations

A boxplot containing the sum capacity for every antenna configuration average over all user positions is shown in Fig. 6.6. Each box in the figure contains the sum capacity of a specific number of antennas removed, i.e. box number 1 contains the sum capacity for all 12 different antenna combinations when 1 antenna is removed. This is repeated up to the removal of 8 antennas, therefore all combinations are included. In Fig. 6.6 two plots are presented. These are the same data but with a difference in scale on the y-axis. Fig. 6.6a shows the data with the same scale in

order to present the difference in magnitude of the capacity, and Fig. 6.6b is for a clearer visualisation of C-MIMO. The equivalent figure for the indoor simulation is Fig 4.7.

In Fig. 6.6 it can be seen that there is a significant difference in sum capacity between C-MIMO and D-MIMO. This means that to achieve a given sum capacity, more antennas can be removed for D-MIMO than C-MIMO. There is a larger variation in the D-MIMO case, this is due to the spatial diversity and the dependence on which antenna that is removed. The variation in C-MIMO is due to constructive and destructive interference when combining the complex impulse responses. Which specific antenna is removed does not affect the coverage since they are located closely together.

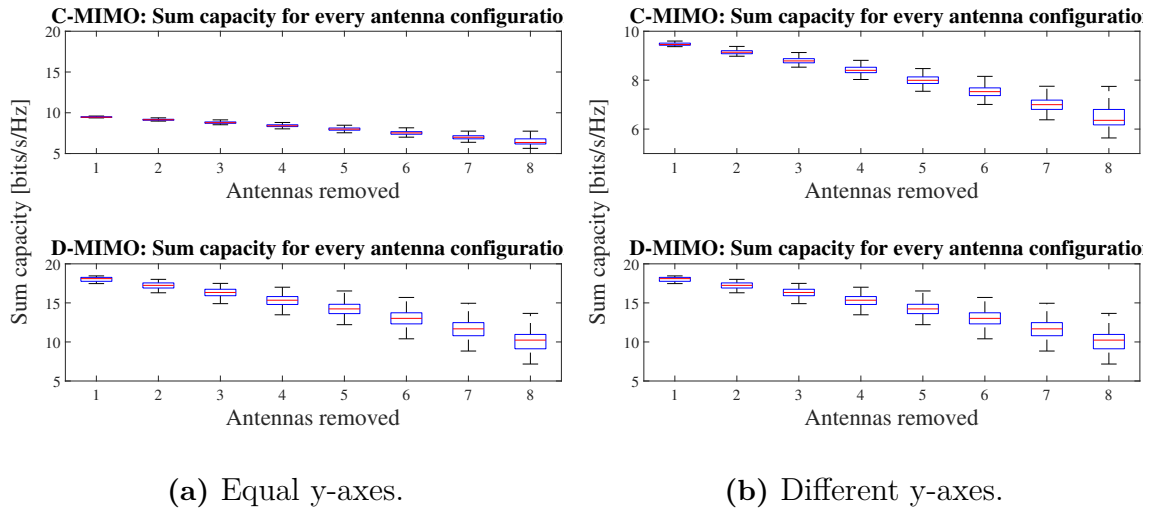


Figure 6.6: Boxplot showing the average total sum capacity for all user and antenna combinations for both C-MIMO and D-MIMO. The x-axis shows the number of antennas removed. The y-axis is the average of the total sum capacity for all user combinations with the red line being the median.

For both systems, the trend is a decrease in capacity when removing antennas which is what is expected since the received power of the incoming signals would be less. It can be seen that C-MIMO has a smaller decline in sum capacity. This means that the system is less sensitive in terms of removing antennas compared to using all 12 antennas. However, while C-MIMO is less affected by removal of antennas, D-MIMO still provides a larger average sum capacity.

6.6 Discussion

The results in this outdoor study is what was expected and it shows similar trends as the indoor simulations, accounted for in Chapter 4. Overall, the D-MIMO system provided better coverage, higher capacity and more received power. This is because the spatially separated transmitter antennas reach users that would otherwise be

affected by shadowing in the C-MIMO case. When the antennas are spatially separate from each other, the channels can be seen as independent from each other which leads to a better conditioned channel matrix and higher capacity.

When removing antennas the outdoor simulation shows same pattern as the indoor simulation. However, there is a larger difference between D-MIMO and C-MIMO in the outdoor case. A probable reason for this is the significantly larger distances in this model which affects C-MIMO more.

There are no major differences between the indoor and outdoor results other than the magnitude of the received power. The received power in the outdoor scenario is in the range of -100 to -55 dBm while in the indoor scenario it is in the range of -70 to -30 dBm. The difference in received power is due to the larger distances in this simulation and therefore an increasing path loss. In the outdoor environment there are mostly line of sight propagation with some ground reflection. This could be compared to the indoor scenario where there are more reflection surfaces. This difference will affect the magnitude of the received power in the outdoor environment negatively.

This study was performed at the end of this project. Due to lack of time the level of detail in the outdoor model is not as high as in the indoor model. For instance, the outdoor model does not contain details such as trees or smaller structures and the houses are modelled as boxes without windows. If more time could be spent on this study more details would have been implemented for a more reliable simulation.

In the indoor study there were measurements performed in the same environment and could therefore act as a reference when building the simulation model. In the outdoor case, no such measurements have been performed. Future work in this study would be to perform measurements in order to verify the results. There is also more possibilities to vary the antenna placement in this environment since the area is larger. Future work would also include constructing a more detailed model of the environment.

7

Conclusion

By simulating an office environment the aim was to study the capacity of a D-MIMO system and compare the results to testbed measurements performed in the same environment. The aim was also to investigate the accuracy of a simulation and the possibility of implementing this method in other scenarios while still achieving reliable results. This thesis shows that similar results, as from the testbed measurements, can be achieved in a simulation. The simulations show the same trends as the measurements, such as the superiority of a D-MIMO system in terms of received power, singular value spread, and capacity, compared to C-MIMO. Both the simulations and measurements indicate a similar pattern along the receiver points, with a decrease of performance at the same locations. In this thesis, it was evident that the simulated C-MIMO system performed better than what the C-MIMO system did in the testbed. However, similar trends are shown between the two with only some differences.

For the indoor environment, the effect of removing antennas in both systems was also investigated. It was shown that the D-MIMO system has a more rapid decrease in capacity than C-MIMO when removing antennas, but D-MIMO can still deliver significantly higher sum capacity. With a comparison of how many antennas that are needed to achieve a reference capacity it has been shown that D-MIMO can with high probability deliver that reference capacity with fewer antennas than C-MIMO. The affect of which antennas are removed is greater for D-MIMO. However, with a strategic removal of antennas, D-MIMO outperforms C-MIMO with less the half the number of antennas in the studied scenario.

The thesis presents preliminary results for a mmWave frequency simulation. This simulation indicated that when using mmWave frequencies the D-MIMO system behaves more similar to C-MIMO than for the 2.365 GHz scenario. The shorter propagation path that comes with higher frequencies decreases the coverage in the locations far from the transmitters and the coverage is not as uniform as with the longer wavelengths. From the study, D-MIMO appears to be most affected of the two systems, with a reduction in mean and increase in variance for the sum capacity. This is a result of the above stated effect when increasing the frequency: loss of coverage means more variation in capacity for some users.

Lastly, an outdoor simulation was performed. The model was produced with the pos-

sibility of performing measurements and is therefore constructed to fit the testbed. The outdoor simulation shows similar behaviour and pattern as for the indoor study, except for the magnitudes of the received power.

Bibliography

- [1] E. J. Oughton, W. Lehr, K. Katsaros, I. Selinis, D. Bublely, and J. Kusuma, “Revisiting wireless internet connectivity: 5g vs wi-fi 6,” 2021.
- [2] K. Sengar, N. Rani, A. Singhal, D. Sharma, S. Verma, and T. Singh, “Study and capacity evaluation of siso, miso and mimo rf wireless communication systems,” *arXiv preprint arXiv:1403.7774*, 2014. [Online]. Available: <https://arxiv.org/pdf/1403.7774.pdf>
- [3] J. Zhang, S. Chen, Y. Lin, J. Zheng, B. Ai, and L. Hanzo, “Cell-free massive mimo: A new next-generation paradigm,” *IEEE Access*, vol. 7, pp. 99 878–99 888, 2019. [Online]. Available: <https://ieeexplore.ieee.org/stamp/stamp.jsp?arnumber=8768014>
- [4] M. Giordani, M. Mezzavilla, and M. Zorzi, “Initial access in 5g mmwave cellular networks,” *IEEE Communications Magazine*, vol. 54, no. 11, pp. 40–47, 2016.
- [5] X. You, D. Wang, and J. Wang, *Distributed MIMO and Cell-free Mobile Communication*. Springer, 2020.
- [6] A. Goldsmith, *Multiple Antennas and Space-Time Communications*. Cambridge University Press, 2005, p. 321–350.
- [7] L. Lu, G. Y. Li, A. L. Swindlehurst, A. Ashikhmin, and R. Zhang, “An overview of massive mimo: Benefits and challenges,” *IEEE Journal of Selected Topics in Signal Processing*, vol. 8, no. 5, pp. 742–758, 2014.
- [8] E. Björnson and L. Sanguinetti, “Cell-free versus cellular massive mimo: What processing is needed for cell-free to win?” in *2019 IEEE 20th International Workshop on Signal Processing Advances in Wireless Communications (SPAWC)*, 2019, pp. 1–5.
- [9] H. Q. Ngo, A. Ashikhmin, H. Yang, E. G. Larsson, and T. L. Marzetta, “Cell-free massive mimo versus small cells,” *IEEE Transactions on Wireless Communications*, vol. 16, no. 3, pp. 1834–1850, 2017. [Online]. Available: <https://ieeexplore.ieee.org/stamp/stamp.jsp?tp=&arnumber=7827017>

- [10] D. Wang, Y. Zhang, H. Wei, X. You, X. Gao, and J. Wang, “An overview of transmission theory and techniques of large-scale antenna systems for 5g wireless communications,” *Science China Information Sciences*, vol. 59, no. 8, pp. 1–18, 2016.
- [11] G. Interdonato, *Cell-Free Massive MIMO: Scalability, Signal Processing and Power Control*. Linköping University Electronic Press, 2020, vol. 2090.
- [12] I. C. Sezgin, M. Dahlgren, T. Eriksson, M. Coldrey, C. Larsson, J. Gustavsson, and C. Fager, “A low-complexity distributed-mimo testbed based on high-speed sigma-delta-over-fiber,” *IEEE Transactions on Microwave Theory and Techniques*, vol. 67, no. 7, pp. 2861–2872, 2019.
- [13] Wireless InSite,v.3.3.5, [Software], PA, USA: Remcom. [Online]. Available: <https://www.remcom.com/wireless-insite-em-propagation-software>
- [14] I. C. Sezgin, T. Eriksson, J. Gustavsson, and C. Fager, “Evaluation of distributed mimo communication using a low-complexity sigma-delta-over-fiber testbed,” in *2019 IEEE MTT-S International Microwave Symposium (IMS)*. IEEE, 2019, pp. 754–757.
- [15] M. Dahlgren, “Implementing distributed mimo: with sigma-delta-over-fiber,” Master’s thesis, Department of Electrical Engineering, Chalmers University, Gothenburg, Sweden, 2018. [Online]. Available: <https://hdl.handle.net/20.500.12380/256447>
- [16] H. Bao, I. Can Sezgin, S. He Zhongxia, T. Eriksson, and C. Fager, “Automatic distributed mimo testbed for beyond 5g communication experiments,” 2020, accepted for presentation at IEEE International Microwave Symposium, 2021.
- [17] A. Goldsmith, *Wireless communications*. Cambridge: Cambridge university press, 2005.
- [18] T. L. Marzetta and B. M. Hochwald, “Fast transfer of channel state information in wireless systems,” *IEEE Transactions on Signal Processing*, vol. 54, no. 8, pp. 1268–1278, 2006.
- [19] E. T. . 101, “Lte; evolved universal terrestrial radio access (e-utra); user equipment (ue) radio transmission and reception (3gpp ts 36.101 version 14.3.0 release 14),” 2017.
- [20] S. Rajagopal, S. Abu-Surra, and M. Malmirchegini, “Channel feasibility for outdoor non-line-of-sight mmwave mobile communication,” in *2012 IEEE vehicular technology conference (VTC Fall)*. IEEE, 2012, pp. 1–6.
- [21] D. Tse and P. Viswanath, *Fundamentals of wireless communication*. Cambridge: Cambridge university press, 2005.

- [22] J. R. Barry, E. A. Lee, and D. G. Messerschmitt, *Digital communication*. Springer Science & Business Media, 2012.
- [23] S. Tiiri, J. Ylioinas, M. Myllyla, and M. Juntti, "Implementation of the least squares channel estimation algorithm for mimo-ofdm systems," in *Proc. of the International ITG Workshop on Smart Antennas (WSA 2009)*, 2009, pp. 16–18.
- [24] X. Gao, O. Edfors, F. Rusek, and F. Tufvesson, "Massive mimo performance evaluation based on measured propagation data," *IEEE Transactions on Wireless Communications*, vol. 14, no. 7, pp. 3899–3911, 2015.
- [25] B. Vucetic and J. Yuan, *Space-time coding*. John Wiley & Sons, 2003, ch. 1, pp. 4–8.
- [26] X.-H. You, D.-M. Wang, B. Sheng, X.-Q. Gao, X.-S. Zhao, and M. Chen, "Cooperative distributed antenna systems for mobile communications [coordinated and distributed mimo]," *IEEE Wireless Communications*, vol. 17, no. 3, pp. 35–43, 2010. [Online]. Available: https://ieeexplore.ieee.org/stamp/stamp.jsp?arnumber=7421222&casa_token=0BxMTzgO7nYAAAAA:5_bL5g3hs6XW8tyb1EStiu_6N5cDkzqHpaRhYSSDLkCnjbHVFO8L289QcXexhdd8V4jfg1do&tag=1
- [27] V. Jungnickel, S. Jaeckel, L. Thiele, L. Jiang, U. Kruger, A. Brylka, and C. Von Helmolt, "Capacity measurements in a cooperative mimo network," *IEEE transactions on vehicular technology*, vol. 58, no. 5, pp. 2392–2405, 2008. [Online]. Available: https://ieeexplore.ieee.org/stamp/stamp.jsp?arnumber=4694097&casa_token=74X8EecYbMcAAAAA:K3Yk5E4d_g3tvczrn7N0qXCbGOTjklmrpSRblsHCuq2453o8EbKkVVUYwJdpUEk9b-VPirPl
- [28] H. Dai, "Distributed versus co-located mimo systems with correlated fading and shadowing," in *2006 IEEE International Conference on Acoustics Speech and Signal Processing Proceedings*, vol. 4. IEEE, 2006, pp. IV–IV. [Online]. Available: https://ieeexplore.ieee.org/stamp/stamp.jsp?arnumber=1661030&casa_token=IoxLXRI3QGgAAAAA:0jEj0xzOvGLq_u5ZA-yrhhdgPTmp1Za3TbNqhwj1TX7Syl_iAfEnteUuaLIH37U3aPVLWl0
- [29] P.-S. Kildal, *Foundations of antenna engineering: a unified approach for line-of-sight and multipath*. Artech House, 2015, ch. 2, pp. 61–63.
- [30] VERT2440 Specification For Approval, Austin, United States of America: Ettus Research LLC, 2011. [Online]. Available: https://kb.ettus.com/images/9/9e/ettus_research_vert2450_datasheet.pdf
- [31] Z. Yun and M. F. Iskander, "Ray tracing for radio propagation modeling: Principles and applications," *IEEE Access*, vol. 3, pp. 1089–1100, 2015.
- [32] L. M. Pessoa, J. S. Tavares, D. Coelho, and H. M. Salgado, "Experimental evaluation of a digitized fiber-wireless system employing sigma delta

modulation,” *Opt. Express*, vol. 22, no. 14, pp. 17 508–17 523, Jul 2014. [Online]. Available: <http://www.opticsexpress.org/abstract.cfm?URI=oe-22-14-17508>

- [33] J. Mao, J. Gao, Y. Liu, and G. Xie, “Simplified semi-orthogonal user selection for mu-mimo systems with zfbf,” *IEEE Wireless Communications Letters*, vol. 1, no. 1, pp. 42–45, 2012.
- [34] OpenStreetMap contributors, “Planet dump retrieved from <https://planet.osm.org>,” <https://www.openstreetmap.org>, 2021.
- [35] Wireless InSite Reference Manual, v.3.3.5, State College, United States of America: Remcom, 2020.

A

Example Output from Wireless InSite

Below is part of an output text file from Wireless InSite. This text file contains the impulse response from one transmitter to all active receivers. In this file the transmitter in question is transmitter 1 and there are 724 active receivers. For each receiver, the simulation includes the impulse response to 25 paths each. The example below has been shortened and only 3 receivers are presented.

The first five rows, beginning with a hashtag, can be explained as follows. First, active transmitter is accounted for. The 3 in “Tx: 3” refers to the ID of the transmitter in Wireless InSite. In “D-MIMO 1 - Point 1” D-MIMO 1 is the chosen name of the transmitter and Point 1 refers to that it is transmitter 1 in that set of transmitter antennas. The same way for the second row, the 1 in “RX: 1” refers to the ID of the receiver in wireless InSite and “RX set” is the given name of the receiver. The third row refers to the number of active receiver points, i.e. 724. The “receiver point number” and “number of paths for this point” is first 1 and 25, then 2 and 25, and so on until it reaches 724 and 25. Finally, the path number, phase value, mean time of arrival and received power are the names of the columns of which the data is given in.

```
# <Transmitter Set: Tx: 3 D-MIMO 1 - Point 1>
# <Receiver Set: Rx: 1 RX set >
# <number of receiver points>
# <receiver point number> <number of paths for this point>
# <path number> <phase value(deg)> <mean time of arrival(sec)>
<received power(dBm)>
  724
  1 25
  1 -15.7679 2.33073e-07 -104.149
  2 125.137 3.12166e-07 -111.143
  3 143.153 3.60554e-07 -112.643
  4 -140.925 1.81886e-07 -112.931
  5 -91.0247 2.90995e-07 -114.03
  6 8.65065 6.38454e-07 -115.464
```

7 -49.7873 2.29127e-07 -116.391
8 114.778 3.58318e-07 -117.224
9 -127.989 3.32963e-07 -118.355
10 -58.4059 2.43451e-07 -118.903
11 147.019 6.40192e-07 -120.237
12 105.388 1.98873e-07 -121.47
13 -102.743 3.39911e-07 -123.911
14 57.0516 3.65786e-07 -124.748
15 -90.9678 3.63154e-07 -125.16
16 131.342 4.1958e-07 -127.48
17 -113.638 1.98495e-07 -128.137
18 140.156 3.61875e-07 -129.561
19 -140.362 2.38481e-07 -130.048
20 64.0941 3.16241e-07 -130.466
21 146.287 3.35811e-07 -130.718
22 -108.151 2.60223e-07 -131.515
23 138.348 3.2478e-07 -131.677
24 48.2564 1.81228e-07 -131.703
25 -67.2675 2.63037e-07 -132.284

2 25

1 6.87538 2.21464e-07 -94.7709
2 52.7492 2.28781e-07 -103.1
3 -64.9416 2.27864e-07 -108.948
4 44.479 3.08888e-07 -111.261
5 57.1044 2.8745e-07 -113.51
6 -36.5263 3.55537e-07 -114.678
7 31.5748 6.24531e-07 -115.499
8 87.7083 2.8853e-07 -116.144
9 45.1785 2.39117e-07 -117.212
10 31.4687 2.61749e-07 -118.921
11 -87.8593 2.40674e-07 -120.293
12 8.99149 2.55793e-07 -120.796
13 -50.6614 3.68669e-07 -121.026
14 159.596 3.34528e-07 -121.123
15 30.3989 1.97693e-07 -121.141
16 -151.487 2.29397e-07 -122.525
17 -29.4838 3.62912e-07 -122.553
18 -1.05947 4.17261e-07 -123.084
19 -112.732 2.56144e-07 -126.36
20 -75.1394 2.74418e-07 -127.129
21 -159.918 2.79571e-07 -127.591
22 -42.488 2.36014e-07 -127.652
23 149.812 1.97341e-07 -128.026
24 -37.599 3.59122e-07 -128.671
25 131.791 2.55219e-07 -128.885

3 25

1 13.6348 2.20615e-07 -95.0813
2 168.724 2.24856e-07 -102.238
3 178.096 2.88424e-07 -102.344
4 -43.0254 2.28899e-07 -103.886
5 -158.95 2.73805e-07 -105.681
6 -78.8677 2.27038e-07 -109.203
7 3.72197 2.78453e-07 -110.151
8 60.6516 2.9723e-07 -112.203
9 -59.6418 2.84216e-07 -113.063
10 -47.088 3.5302e-07 -114.76
11 143.569 2.51679e-07 -115.237
12 -107.645 2.91085e-07 -115.47
13 -148.704 2.35131e-07 -115.548
14 -73.6832 3.50308e-07 -117.143
15 48.299 2.3553e-07 -118.237
16 43.9371 2.02749e-07 -118.269
17 72.1579 1.73229e-07 -118.976
18 -102.325 3.16924e-07 -119.338
19 27.7664 2.38014e-07 -121.163
20 -106.108 3.66203e-07 -121.255
21 108.688 2.7897e-07 -122.303
22 -167.692 2.02996e-07 -122.324
23 45.3628 3.60295e-07 -122.497
24 -18.1944 4.15173e-07 -123.317
25 91.2368 3.56232e-07 -123.525

B

Complement to Indoor Environment Study

B.1 Received Power Without Phase

The received power for each receiver point in the indoor environment when not including the phase can be seen in Fig. B.1. The figure corresponds to the study using 2.365 GHz frequency.

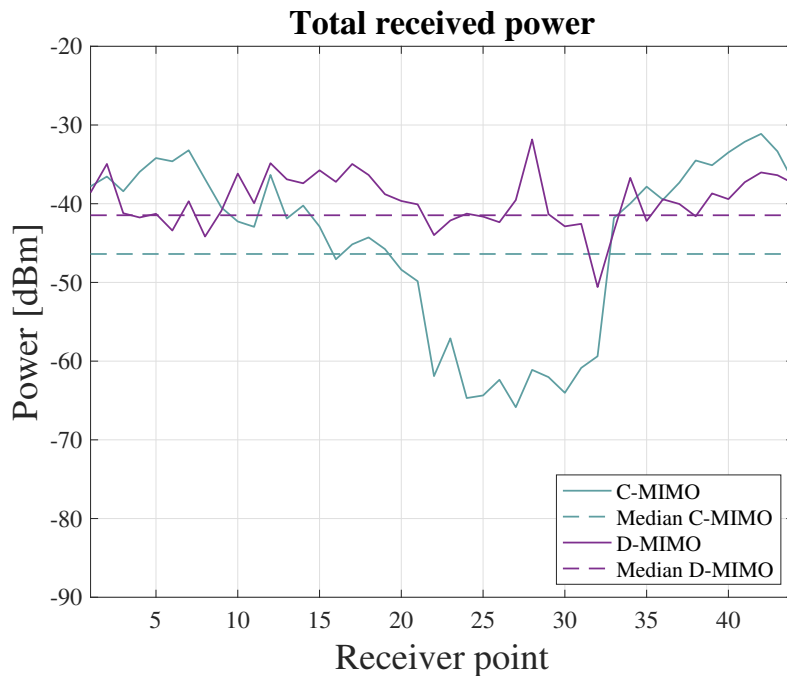


Figure B.1: The received power for the indoor environment when not including the phase.

B.2 Sum Capacity With Different SNR

The sum capacities for D-MIMO and C-MIMO with different SNR settings are shown in Fig. B.2

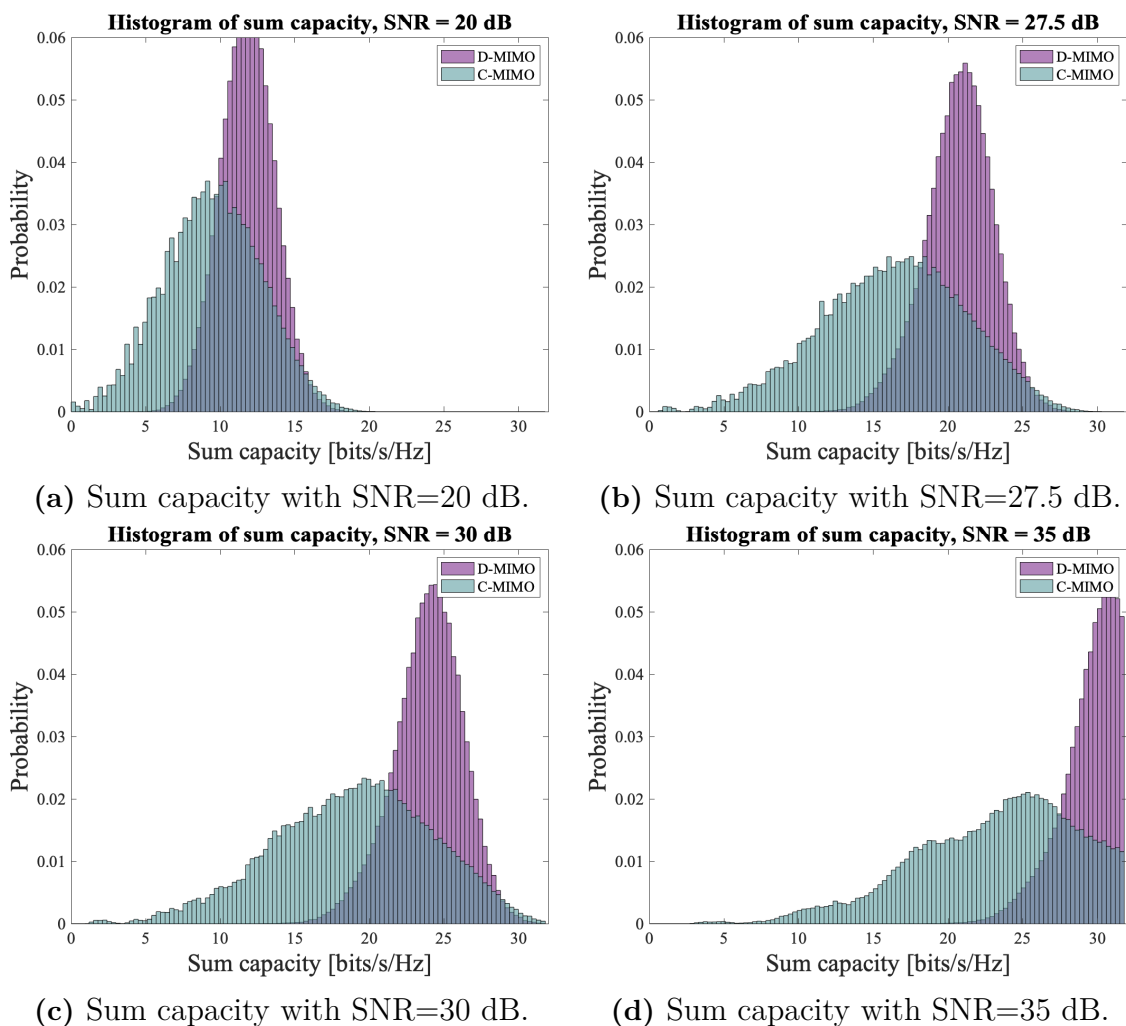


Figure B.2: The sum capacity shown with different SNR values.



CHALMERS
UNIVERSITY OF TECHNOLOGY